CU-CAS-05-06

CENTER FOR AEROSPACE STRUCTURES

SUPERNATURAL QUAD4: A TEMPLATE FORMULATION

by

C. A. Felippa

December 2005

COLLEGE OF ENGINEERING
UNIVERSITY OF COLORADO
CAMPUS BOX 429
BOULDER, COLORADO 80309

Supernatural Quad4: A Template Formulation

C. A. Felippa

Department of Aerospace Engineering Sciences
and Center for Aerospace Structures
University of Colorado, Campus Box 429
Boulder, Colorado 80309-0429, USA

Report No. CU-CAS-05-06

November 2005

Contributed to the J. H. Argyris Memorial Issue of *Computer Methods in Applied Mechanics and Engineering*. To appear 2006.

Contributed to Special CMAME Issue in Memory of J. H. Argyris

SUPERNATURAL QUAD4: A TEMPLATE FORMULATION

Carlos A. Felippa

Department of Aerospace Engineering Sciences
and Center for Aerospace Structures
University of Colorado, CB 429
Boulder, CO 80309-0429, USA
Email: carlos.felippa@colorado.edu
Web page: http://caswww.colorado.edu/Felippa.d/FelippaHome.d/Home.html

Abstract. A universal template for a 4-node quadrilateral in plane stress is constructed using a combination of old and new techniques. The use of natural quantities, strongly advocated by J. H. Argyris since his *Continua and Discontinua* 1965 exposition, is further expanded. The qualifier 'supernatural' means that all governing equations: kinematic, constitutive and equilibrium, are expressed in both Cartesian and natural forms. These two sets are used to build different components of the template. With timely help from a computer algebra system, a template that include all possible quadrilateral elements that pass the Individual Element Test of Bergan and Hanssen emerges. It yields an infinite number of hitherto undiscovered instances that may be customized to fit special needs. A striking example is the construction of a two-trapezoid macroelement that is bending exact about one direction, for any amount of distortion. This concludes a five decade search that begins with the formulation of the wing-cover rectangular panel in Argyris' 1954 seminal serial on *Energy Methods and Structural Analysis*.

Key words: finite elements, templates, natural fields, natural equations, quadrilateral panel, Free Formulation, patch test, individual element test.

TABLE OF CONTENTS

§1. Introduction

This paper considers the 4-node, 8-DOF quadrilateral element to model a thin flat plate in plane stress. This will be called the *quadrilateral panel* for brevity. The main goal is to construct the best possible element of this type, customized to fit stated needs, using templates. Achieving this goal would conclude a long and seminal road started by John Argyris in his celebrated 1954 serial [3] and pursued by many investigators over five decades. A historical overview pertaining to the evolution of this element type as a driver for finite element technology is provided in Section 7.

§2. Governing Equations

Consider a thin, elastic, homogeneous flat plate in plane stress. This is idealized as a two-dimensional boundary value problem idealized as sketched in Figure 1. The two-dimensional mathematical model of the plate occupies domain Ω with boundary Γ. The $\{x, y, z\}$ axes are chosen as indicated in that figure.

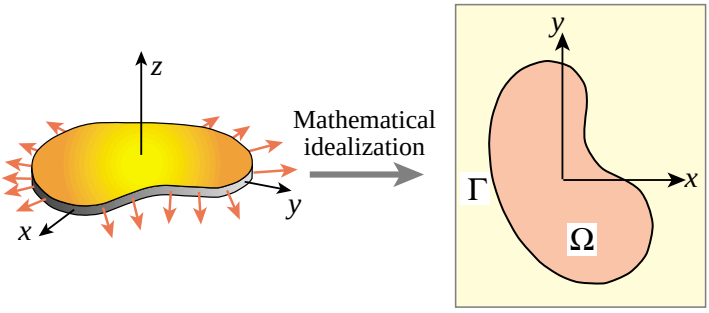

FIGURE 1. A thin plate in plane stress.

The notation used for internal fields is summarized in Figure 2. The in-plane displacements are $\{u_x, u_y\}$, the associated strains are $\{e_{xx}, e_{yy}, e_{xy}\}$ and the in-plane (membrane) stresses are $\{\sigma_{xx}, \sigma_{yy}, \sigma_{xy}\}$. Prescribed in-plane body forces are $\{b_x, b_y\}$, but these will be set to zero in derivations that involve equilibrium equations. Prescribed displacements and surface tractions are denoted by $\{\hat{u}_x, \hat{u}_y\}$ and $\{\hat{t}_x, \hat{t}_y\}$ respectively.

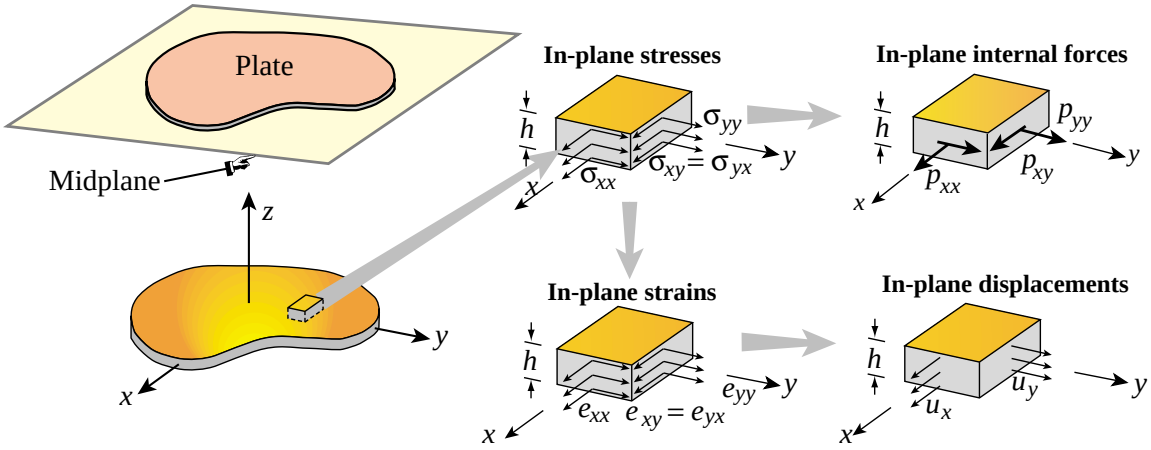

FIGURE 2. Notation used for thin plate in plane stress.

All fields are considered uniform through the plate thickness h. If h is a function of $\{x, y\}$, it should vary only gradually so that the two-dimensional plane stress idealization remains valid.

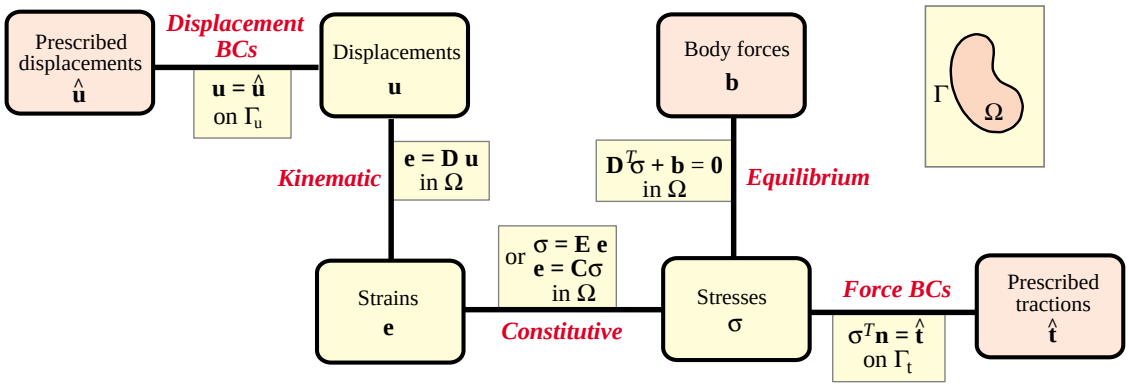

FIGURE 3. Tonti diagram for strong form of the plane stress problem.

The governing plane-stress elasticity equations are

$$\begin{bmatrix} e_{xx} \\ e_{yy} \\ 2e_{xy} \end{bmatrix} = \begin{bmatrix} \partial/\partial x & 0 \\ 0 & \partial/\partial y \\ \partial/\partial y & \partial/\partial x \end{bmatrix} \begin{bmatrix} u_x \\ u_y \end{bmatrix}, \qquad \begin{bmatrix} \sigma_{xx} \\ \sigma_{yy} \\ \sigma_{xy} \end{bmatrix} = \begin{bmatrix} E_{11} & E_{12} & E_{13} \\ E_{12} & E_{22} & E_{23} \\ E_{13} & E_{23} & E_{33} \end{bmatrix} \begin{bmatrix} e_{xx} \\ e_{yy} \\ 2e_{xy} \end{bmatrix},$$
$$\begin{bmatrix} \partial/\partial x & 0 & \partial/\partial y \\ 0 & \partial/\partial y & \partial/\partial x \end{bmatrix} \begin{bmatrix} \sigma_{xx} \\ \sigma_{yy} \\ \sigma_{xy} \end{bmatrix} + \begin{bmatrix} b_x \\ b_y \end{bmatrix} = \begin{bmatrix} 0 \\ 0 \end{bmatrix}. \tag{1}$$

The compact matrix version of (1) is

$$\mathbf{e} = \mathbf{D}\,\mathbf{u}, \qquad \boldsymbol{\sigma} = \mathbf{E}\,\mathbf{e}, \qquad \mathbf{D}^T\,\boldsymbol{\sigma} + \mathbf{b} = \mathbf{0}, \tag{2}$$

in which $\mathbf{E}$ is the plane stress elasticity matrix. Assuming this to be nonsingular, the inverse of $\boldsymbol{\sigma} = \mathbf{E}\,\mathbf{e}$ is

$$\begin{bmatrix} e_{xx} \\ e_{yy} \\ 2e_{xy} \end{bmatrix} = \begin{bmatrix} C_{11} & C_{12} & C_{13} \\ C_{12} & C_{22} & C_{23} \\ C_{13} & C_{23} & C_{33} \end{bmatrix} \begin{bmatrix} \sigma_{xx} \\ \sigma_{yy} \\ \sigma_{xy} \end{bmatrix}, \quad \text{or} \quad \mathbf{e} = \mathbf{C}\,\boldsymbol{\sigma}, \tag{3}$$

where $\mathbf{C} = \mathbf{E}^{-1}$ is the matrix of elastic compliances. These equations are graphically represented in the strong-form Tonti diagram of Figure 3.

§3. The Quadrilateral Panel

The focus of the paper is the 4-noded *quadrilateral panel element*. This configuration is depicted in Figure 4. The element occupies the domain Ω^e and has boundary Γ^e. The thickness and constitutive properties, defined by the $\mathbf{E}$ or $\mathbf{C}$ matrices, are constant over the element. The corner coordinates are $\{x_i, y_i\}$, $i = 1, 2, 3, 4$. Abbreviations $x_{ij} = x_i - x_j$ and $y_{ij} = y_i - y_j$ are used for node coordinate differences.

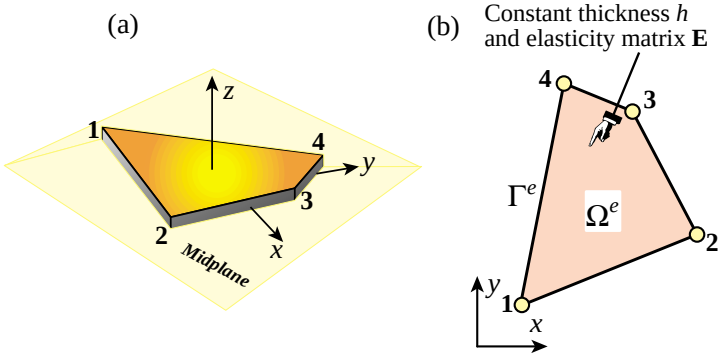

FIGURE 4. The 4-node quadrilateral panel.

Table 1. Side-bySide Cartesian and Natural Notation

Quantity	Cartesian form		Natural form	
	Components	Matrix	Components	Matrix
Coordinate array	$\{x, y\}$	$\mathbf{x}$	$\{\xi, \eta\}$	$\boldsymbol{\xi}$
Position vector of point P	$P(x, y)$	$\vec{\mathbf{x}}$	$P(\xi, \eta)$	$\boldsymbol{\xi}$
Base vectors	$\{1, 0\}, \{0, 1\}$	$\mathbf{a}_x, \mathbf{a}_y$	See eqn (6)	$\mathbf{a}_1, \mathbf{a}_2$
Displacement field	$\{u_x, u_y\}$	$\vec{\mathbf{u}}$	$\{\breve{u}_\xi, \breve{u}_\eta\}$	$\breve{\mathbf{u}}$
Strain field	$\{e_{xx}, e_{yy}, g_{xy}\}$	$\mathbf{e}$	$\{\breve{e}_{\xi\xi}, \breve{e}_{\eta\eta}, \breve{g}_{\xi\eta}\}$	$\breve{\mathbf{e}}$
Stress field	$\{\sigma_{xx}, \sigma_{yy}, \sigma_{xy}\}$	$\mathbf{e}$	$\{\breve{\sigma}_{\xi\xi}, \breve{\sigma}_{\eta\eta}, \breve{\sigma}_{xi\eta}\}$	$\breve{\boldsymbol{\sigma}}$
Elastic moduli	$\{E_{11}, \ldots, E_{33}\}$	$\mathbf{E}$	$\{\breve{E}_{11}, \ldots, \breve{E}_{33}\}$	$\breve{\mathbf{E}}$
Elastic compliances	$\{C_{11}, \ldots, C_{33}\}$	$\mathbf{C}$	$\{\breve{C}_{11}, \ldots, \breve{C}_{33}\}$	$\breve{\mathbf{C}}$
Elem node coordinates	$\{x_1, y_1, \ldots x_4, y_4\}$	$\mathbf{x}^e$	$\{\xi_1, \eta_1, \ldots \xi_4, \eta_4\}$	ξ^e
Elem node displacements	$\{u_{x1}, u_{y1}, \ldots u_{x4}, u_{y4}\}$	$\mathbf{u}^e$	$\{\breve{u}_{\xi 1}, \breve{u}_{\eta 1}, \ldots \breve{u}_{\xi 4}, \breve{u}_{\eta 4}\}$	$\breve{\mathbf{u}}^e$
Elem node forces	$\{f_{x1},\ f_{y1}, \ldots\ f_{x4},\ f_{y4}\}$	$\mathbf{f}^e$	$\{\breve{f}_{\xi 1},\ \breve{f}_{\eta 1}, \ldots\ \breve{f}_{\xi 4},\ \breve{f}_{\eta 4}\}$	$\breve{\mathbf{f}}^e$

$\vec{\mathbf{x}}$, $\vec{\mathbf{u}}$ are used when manipulations as a vector object are emphasized.

The element has 8 external (connective) degrees of freedom (DOF). The node displacement and force vectors are configured as

$$\begin{aligned} \mathbf{u}^e &= [\, u_{x1} \quad u_{y1} \quad u_{x2} \quad u_{y2} \quad u_{x3} \quad u_{y3} \quad u_{x4} \quad u_{y4} \,]^T , \\ \mathbf{f}^e &= [\, f_{x1} \quad f_{y1} \quad f_{x2} \quad f_{y2} \quad f_{x3} \quad f_{y3} \quad f_{x4} \quad f_{y4} \,]^T . \end{aligned} \tag{4}$$

The formulation of the stiffness template is significantly simplified by working out invariant geometric properties of the quadrilateral. The development is rather lengthly and so is relegated to Appendix A.

§3.1. Natural Displacements

Table 1 summarizes notation used in the sequel for Cartesian and natural quantities. The Cartesian unit base vectors are $\mathbf{i}_x$ and $\mathbf{i}_y$. The natural unit basis vectors at a generic point $P(\xi, \eta)$ are called $\mathbf{a}_1$ and $\mathbf{a}_2$. Denote by ϕ_1 and ϕ_2 the angles from $+x$ to $\mathbf{a}_1$ and from $+y$ to $\mathbf{a}_2$, as illustrated in Figure 5(a). (Positive if counter-clockwise; both angles shown in the figure are negative.) Then

$$\begin{aligned} \mathbf{a}_1 &= (J_{11}/J_1)\,\mathbf{i}_x + (J_{12}/J_1)\,\mathbf{i}_y = \quad \cos\phi_1\,\mathbf{i}_x + \sin\phi_1\,\mathbf{i}_y, \\ \mathbf{a}_2 &= (J_{21}/J_2)\,\mathbf{i}_x + (J_{22}/J_2)\,\mathbf{i}_y = -\sin\phi_2\,\mathbf{i}_x + \cos\phi_2,\mathbf{i}_y, \end{aligned} \tag{5}$$

where the $J's$ are defined in Appendix Section A.2. The natural (covariant) displacement components are the projections of the physical displacement vector $\vec{\mathbf{u}}(\xi, \eta)$ at $P(\xi, \eta)$ on the natural base vectors: $\breve{u}_\xi = \vec{\mathbf{u}} \cdot \mathbf{a}_1$ and $\breve{u}_\eta = \vec{\mathbf{u}} \cdot \mathbf{a}_2$. See Figure 5(b). In matrix form

$$\breve{\mathbf{u}} = \begin{bmatrix} \breve{u}_\xi \\ \breve{u}_\eta \end{bmatrix} = \begin{bmatrix} J_{11}/J_1 & J_{12}/J_1 \\ J_{21}/J_2 & J_{22}/J_2 \end{bmatrix} \begin{bmatrix} u_x \\ u_y \end{bmatrix} = \begin{bmatrix} \cos\phi_1 & \sin\phi_1 \\ -\sin\phi_2 & \cos\phi_2 \end{bmatrix} \begin{bmatrix} u_x \\ u_y \end{bmatrix} = \mathbf{D}_J\,\mathbf{J}\,\mathbf{u} = \breve{\mathbf{J}}\,\mathbf{u} = \breve{\mathbf{T}}_d^{-1}\mathbf{u}. \tag{6}$$

The inverse is

$$\mathbf{u} = \begin{bmatrix} u_x \\ u_y \end{bmatrix} = \frac{1}{\cos(\phi_1 - \phi_2)} \begin{bmatrix} \cos\phi_2 & -\sin\phi_1 \\ \sin\phi_2 & \cos\phi_1 \end{bmatrix} \begin{bmatrix} \breve{u}_\xi \\ \breve{u}_\eta \end{bmatrix} = \breve{\mathbf{T}}_d\,\breve{\mathbf{u}}. \tag{7}$$

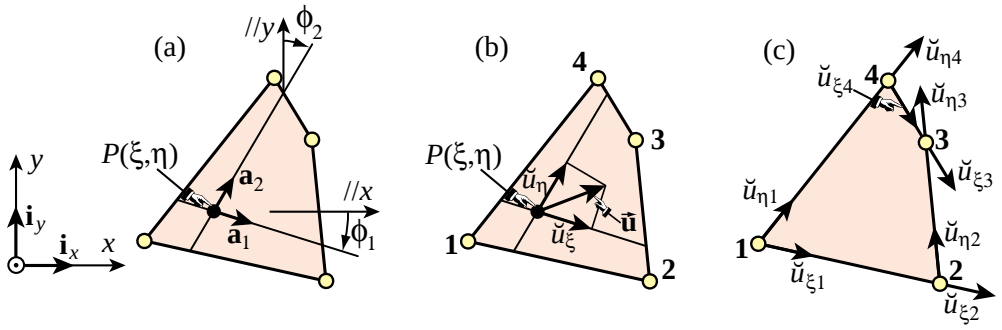

FIGURE 5. Natural displacement field. (a) Base vectors and their angles with $\{x, y\}$ (in the figure both ϕ_1 and ϕ_2 are negative), (b) natural displacement components at an arbitrary point; (c) natural node displacements.

Evaluation of $\breve{u}_\xi$ and $\breve{u}_\eta$ at the nodes gives 8 natural (covariant) node displacements, which are pictured in Figure 5(c). These are collected in array $\breve{\mathbf{u}}^e$. Cartesian and natural node displacements are linked by the transformation matrix

$$\breve{\mathbf{u}}^e = \begin{bmatrix} \breve{u}_{\xi 1} \\ \breve{u}_{\eta 1} \\ \breve{u}_{\xi 2} \\ \breve{u}_{\eta 2} \\ \breve{u}_{\xi 3} \\ \breve{u}_{\eta 3} \\ \breve{u}_{\xi 4} \\ \breve{u}_{\eta 4} \end{bmatrix} = \begin{bmatrix} \frac{x_{21}}{L_{21}} & \frac{y_{21}}{L_{21}} & 0 & 0 & 0 & 0 & 0 & 0 \\ \frac{-x_{14}}{L_{14}} & \frac{-y_{14}}{L_{14}} & 0 & 0 & 0 & 0 & 0 & 0 \\ 0 & 0 & \frac{x_{21}}{L_{21}} & \frac{y_{21}}{L_{21}} & 0 & 0 & 0 & 0 \\ 0 & 0 & \frac{x_{32}}{L_{32}} & \frac{y_{32}}{L_{32}} & 0 & 0 & 0 & 0 \\ 0 & 0 & 0 & 0 & \frac{-x_{43}}{L_{43}} & \frac{-y_{43}}{L_{43}} & 0 & 0 \\ 0 & 0 & 0 & 0 & \frac{x_{32}}{L_{32}} & \frac{y_{32}}{L_{32}} & 0 & 0 \\ 0 & 0 & 0 & 0 & 0 & 0 & \frac{-x_{43}}{L_{43}} & \frac{-y_{43}}{L_{43}} \\ 0 & 0 & 0 & 0 & 0 & 0 & \frac{-x_{14}}{L_{14}} & \frac{-y_{14}}{L_{14}} \end{bmatrix} \begin{bmatrix} u_{x1} \\ u_{y1} \\ u_{x2} \\ u_{y2} \\ u_{x3} \\ u_{y3} \\ u_{x4} \\ u_{y4} \end{bmatrix} \stackrel{\text{def}}{=} \breve{\mathbf{T}}_u^{-1}\, \mathbf{u}^e. \tag{8}$$

with inverse

$$\mathbf{u}^e = \begin{bmatrix} u_{x1} \\ u_{y1} \\ u_{x2} \\ u_{y2} \\ u_{x3} \\ u_{y3} \\ u_{x4} \\ u_{y4} \end{bmatrix} = \tfrac{1}{2} \begin{bmatrix} \frac{-L_{21}y_{14}}{A_{412}} & \frac{-L_{14}y_{21}}{A_{412}} & 0 & 0 & 0 & 0 & 0 & 0 \\ \frac{L_{21}x_{14}}{A_{412}} & \frac{L_{14}x_{21}}{A_{412}} & 0 & 0 & 0 & 0 & 0 & 0 \\ 0 & 0 & \frac{L_{21}y_{32}}{A_{123}} & \frac{-L_{32}y_{21}}{A_{123}} & 0 & 0 & 0 & 0 \\ 0 & 0 & \frac{-L_{21}x_{32}}{A_{123}} & \frac{L_{32}x_{21}}{A_{123}} & 0 & 0 & 0 & 0 \\ 0 & 0 & 0 & 0 & \frac{L_{43}y_{32}}{A_{234}} & \frac{L_{32}y_{43}}{A_{234}} & 0 & 0 \\ 0 & 0 & 0 & 0 & \frac{-L_{43}x_{32}}{A_{234}} & \frac{-L_{32}x_{43}}{A_{234}} & 0 & 0 \\ 0 & 0 & 0 & 0 & 0 & 0 & \frac{-L_{43}y_{14}}{A_{341}} & \frac{L_{14}y_{43}}{A_{341}} \\ 0 & 0 & 0 & 0 & 0 & 0 & \frac{L_{43}x_{14}}{A_{341}} & \frac{-L_{14}x_{43}}{A_{341}} \end{bmatrix} \begin{bmatrix} \breve{u}_{\xi 1} \\ \breve{u}_{\eta 1} \\ \breve{u}_{\xi 2} \\ \breve{u}_{\eta 2} \\ \breve{u}_{\xi 3} \\ \breve{u}_{\eta 3} \\ \breve{u}_{\xi 4} \\ \breve{u}_{\eta 4} \end{bmatrix} = \breve{\mathbf{T}}_u\, \breve{\mathbf{u}}^e. \tag{9}$$

Here L_{ij} is the length of side joining corners i and j whereas areas A_{ijk} are defined in (57).

§3.2. Natural Strains

Following Park and Stanley [47,58], the natural strain components with respect to a *fixed* coordinate basis $\{\mathbf{a}_1, \mathbf{a}_2\}$ are defined by

$$\breve{e}_{\xi\xi} = \frac{1}{J_1}\frac{\bar{\partial}\breve{u}_\xi}{\bar{\partial}\xi}, \quad \breve{e}_{\eta\eta} = \frac{1}{J_2}\frac{\bar{\partial}\breve{u}_\eta}{\bar{\partial}\eta}, \quad \breve{e}_{\eta\xi} = \frac{1}{J_1}\frac{\bar{\partial}\breve{u}_\eta}{\bar{\partial}\xi}, \quad \breve{e}_{\xi\eta} = \frac{1}{J_2}\frac{\bar{\partial}\breve{u}_\xi}{\bar{\partial}\eta}, \quad \breve{\gamma}_{\xi\eta} = \breve{e}_{\xi\eta} + \breve{e}_{\eta\xi}. \tag{10}$$

Here $\bar\partial$ indicates that metric coefficients are "frozen" when taking partial derivatives. For example:

$$\breve{e}_{\xi\xi} = \frac{1}{J_1}\frac{\bar\partial \breve{u}_\xi}{\bar\partial \xi} = \frac{1}{J_1}\left(\frac{J_{11}}{J_1}\frac{\partial u_x}{\partial \xi} + \frac{J_{12}}{J_1}\frac{\partial u_y}{\partial \xi}\right) = \frac{1}{J_1^2}\left(J_{11}^2 e_{xx} + J_{12}^2 e_{yy} + J_{11}J_{12}\gamma_{xy}\right). \tag{11}$$

In operator matrix form:

$$\begin{bmatrix} \breve{e}_{\xi\xi} \\ \breve{e}_{\eta\eta} \\ \breve{\gamma}_{\xi\eta} \end{bmatrix} = \begin{bmatrix} J_1^{-1}(\bar\partial/\bar\partial\xi) & 0 \\ 0 & J_2^{-1}(\bar\partial/\bar\partial\eta) \\ J_2^{-1}(\bar\partial/\bar\partial\eta) & J_1^{-1}(\bar\partial/\bar\partial\xi) \end{bmatrix} \begin{bmatrix} \breve{u}_\xi \\ \breve{u}_\eta \end{bmatrix} \stackrel{\text{def}}{=} \breve{\mathbf{D}}\,\breve{\mathbf{u}}^e, \tag{12}$$

in which $\breve{\mathbf{D}}$ denotes the natural strain-displacement operator. On expanding as typified by (11), the transformation between Cartesian and natural strains can be expressed in matrix form as

$$\begin{aligned} \breve{\mathbf{e}} = \begin{bmatrix} \breve{e}_{\xi\xi} \\ \breve{e}_{\eta\eta} \\ \breve{\gamma}_{\xi\eta} \end{bmatrix} &= \begin{bmatrix} 1/J_1^2 & 0 & 0 \\ 0 & 1/J_2^2 & 0 \\ 0 & 0 & 1/(J_1J_2) \end{bmatrix} \begin{bmatrix} J_{11}^2 & J_{12}^2 & J_{11}\,J_{12} \\ J_{21}^2 & J_{22}^2 & J_{21}\,J_{22} \\ 2J_{11}\,J_{21} & 2J_{12}\,J_{22} & J_{11}J_{22}+J_{12}J_{12} \end{bmatrix} \begin{bmatrix} e_{xx} \\ e_{yy} \\ 2e_{xy} \end{bmatrix} \\ &= \begin{bmatrix} \cos^2\phi_1 & \sin^2\phi_1 & \cos\phi_1\sin\phi_1 \\ \sin^2\phi_2 & \cos^2\phi_2 & -\cos\phi_2\sin\phi_2 \\ -2\cos\phi_1\sin\phi_2 & 2\cos\phi_2\sin\phi_1 & \cos(\phi_1+\phi_2) \end{bmatrix} \mathbf{e} \stackrel{\text{def}}{=} \breve{\mathbf{T}}_e^{-1}\mathbf{e}. \end{aligned} \tag{13}$$

The inverse is

$$\begin{aligned} \begin{bmatrix} e_{xx} \\ e_{yy} \\ 2e_{xy} \end{bmatrix} &= (1/J^2)\begin{bmatrix} J_{22}^2 & J_{12}^2 & -J_{12}\,J_{22} \\ J_{21}^2 & J_{11}^2 & -J_{11}\,J_{21} \\ -2J_{21}\,J_{22} & -2J_{11}\,J_{12} & J_{11}J_{22}+J_{12}J_{21} \end{bmatrix} \begin{bmatrix} J_1^2 & 0 & 0 \\ 0 & J_2^2 & 0 \\ 0 & 0 & J_1J_2 \end{bmatrix} \begin{bmatrix} \breve{e}_{\xi\xi} \\ \breve{e}_{\eta\eta} \\ \breve{\gamma}_{\xi\eta} \end{bmatrix} \\ &= \frac{1}{\cos^2(\phi_1-\phi_2)}\begin{bmatrix} \cos^2\phi_2 & \sin^2\phi_1 & -\cos\phi_2\sin\phi_1 \\ \sin^2\phi_2 & \cos^2\phi_1 & \cos\phi_1\sin\phi_2 \\ \sin 2\phi_2 & -\sin 2\phi_1 & \cos(\phi_1+\phi_2) \end{bmatrix} \begin{bmatrix} \breve{e}_{\xi\xi} \\ \breve{e}_{\eta\eta} \\ \breve{\gamma}_{\xi\eta} \end{bmatrix} = \breve{\mathbf{T}}_e\,\breve{\mathbf{e}}. \end{aligned} \tag{14}$$

in which $J = J_{11}J_{22} - J_{12}J_{21}$. The natural strains (10) do not form a tensor. Some authors have defined tensorial (covariant) natural strains with respect to a moving base-vector system $\{\mathbf{a}_1, \mathbf{a}_2\}$. As noted in [47] that complication is unnecessary as it does not produce better elements. This was confirmed in a recent study of this element type by Lautersztajn and Samuelsson [37].

Since $\mathbf{e} = \mathbf{D}\,\mathbf{u} = \breve{\mathbf{T}}_e\,\breve{\mathbf{e}}$ and $\mathbf{u} = \breve{\mathbf{T}}_d\,\breve{\mathbf{u}}$, eliminating $\mathbf{e}$ and $\mathbf{u}$ yields $\breve{\mathbf{e}} = \breve{\mathbf{T}}_e^{-1}\mathbf{D}\breve{\mathbf{T}}_d\,\breve{\mathbf{u}} \stackrel{\text{def}}{=} \breve{\mathbf{D}}\,\breve{\mathbf{u}}$.Thus $\breve{\mathbf{D}} = \breve{\mathbf{T}}_e^{-1}\mathbf{D}\breve{\mathbf{T}}_d$. Solving for $\mathbf{D}$ in terms of $\breve{\mathbf{D}}$ yields

$$\mathbf{D} = \mathbf{T}_e\,\breve{\mathbf{D}}\,\mathbf{T}_d^{-1} = \frac{1}{J}\begin{bmatrix} J_{22}\dfrac{\bar\partial}{\bar\partial\xi} - J_{12}\dfrac{\bar\partial}{\bar\partial\eta} & 0 \\ 0 & -J_{21}\dfrac{\bar\partial}{\bar\partial\xi} + J_{11}\dfrac{\bar\partial}{\bar\partial\eta} \\ -J_{21}\dfrac{\bar\partial}{\bar\partial\xi} + J_{11}\dfrac{\bar\partial}{\bar\partial\eta} & J_{22}\dfrac{\bar\partial}{\bar\partial\xi} - J_{12}\dfrac{\bar\partial}{\bar\partial\eta} \end{bmatrix} \equiv \begin{bmatrix} \partial/\partial x & 0 \\ 0 & \partial/\partial y \\ \partial/\partial y & \partial/\partial x \end{bmatrix} \tag{15}$$

The entries in (15) gives the expression of $\partial/\partial x$ and $\partial/\partial y$ in fixed-base-vector natural coordinates. If moving base vectors were adopted, $\{\xi, \eta\}$ partials of the metric coefficients would appear.

§3.3. Natural Strain-Displacement Equations

At this juncture two paths may be followed to construct element-level strain-displacement relations in natural coordinates:

(1) Interpolate natural displacements isoparametrically and apply (12).

(2) Interpolate Cartesian displacements isoparametrically and transform Cartesian to natural strains.

The first approach leads to natural displacements that violate interelement compatibility because metric coefficients typically jump there. See Figure 6. This is a consequence of natural node displacements being generally misaligned when one considers adjacent elements.

The second approach retains interelement continuity and is the one followed here. The resulting natural strain field will not generally satisfy differential compatibility, but it is precisely that "compatibility relaxation" that makes possible the construction of high performance elements.

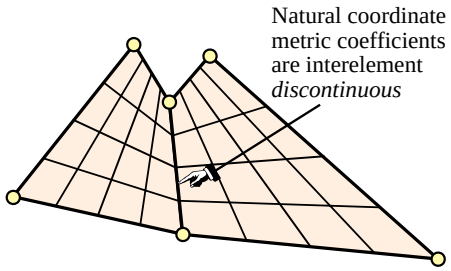

FIGURE 6. Jump of natural metric at an interelement boundary.

The strain displacement matrix that relates Cartesian strains $\mathbf{e} = [\, e_{xx}, e_{yy}, 2e_{xy}\,]^T$ to Cartesian node displacements $\mathbf{u}^e$ is $\mathbf{e}_{iso} = \mathbf{B}_{iso}\,\mathbf{u}^e$, where the subscript 'iso' means that the Cartesian displacements $u_x(\xi,\eta)$ and $u_y(\xi,\eta)$ are interpolated isoparametrically by the bilinear shape functions N_i of (55). The well known expression of $\mathbf{B}_{iso}$ is

$$\mathbf{B}_{iso} = \mathbf{B}_c + \mathbf{B}_h = \mathbf{B}_c + \mathbf{B}_d + \mathbf{B}_\xi\,\xi + \mathbf{B}_\eta\,\eta, \tag{16}$$

where

$$\begin{aligned}
\mathbf{B}_c &= \frac{1}{2A}\begin{bmatrix} y_{24} & 0 & y_{31} & 0 & y_{42} & 0 & y_{13} & 0 \\ 0 & x_{42} & 0 & x_{13} & 0 & x_{24} & 0 & x_{31} \\ x_{42} & y_{24} & x_{13} & y_{31} & x_{24} & y_{42} & x_{31} & y_{13} \end{bmatrix}, \quad \mathbf{B}_d = \left(\frac{A}{4J} - 1\right)\mathbf{B}_c, \\
\mathbf{B}_\xi &= \frac{1}{8J}\begin{bmatrix} y_{43} & 0 & y_{34} & 0 & y_{12} & 0 & y_{21} & 0 \\ 0 & x_{34} & 0 & x_{43} & 0 & x_{21} & 0 & x_{12} \\ x_{34} & y_{43} & x_{43} & y_{34} & x_{21} & y_{12} & x_{12} & y_{21} \end{bmatrix}, \\
\mathbf{B}_\eta &= \frac{1}{8J}\begin{bmatrix} y_{32} & 0 & y_{14} & 0 & y_{41} & 0 & y_{23} & 0 \\ 0 & x_{23} & 0 & x_{41} & 0 & x_{14} & 0 & x_{32} \\ x_{23} & y_{32} & x_{41} & y_{14} & x_{14} & y_{41} & x_{32} & y_{23} \end{bmatrix}.
\end{aligned} \tag{17}$$

in which $J = J_{11}J_{22} - J_{12}J_{21}$, and A is the signed quadrilateral area given by (56). Note that $\mathbf{B}_c$ is the mean value of $\mathbf{B}_{iso}$ in the sense that

$$\frac{1}{A}\int_{\Omega^e} \mathbf{B}_{iso}\, d\Omega = \frac{1}{A}\int_{\Omega^e} \mathbf{B}_{iso}\, J\, d\xi\, d\eta = \mathbf{B}_c, \tag{18}$$

exactly for any geometry. Passing to natural coordinates: $\breve{\mathbf{e}} = \breve{\mathbf{T}}_e^{-1}\,\mathbf{e} = \breve{\mathbf{T}}_e^{-1}\,\mathbf{B}_{iso}\,\mathbf{u}^e = \breve{\mathbf{T}}_e^{-1}\mathbf{B}_{iso}\breve{\mathbf{T}}_u\,\breve{\mathbf{u}}^e \stackrel{\text{def}}{=} \breve{\mathbf{B}}_{iso}\,\breve{\mathbf{u}}^e$. Consequently $\breve{\mathbf{B}}_{iso} = \breve{\mathbf{T}}_e^{-1}\,\mathbf{B}_{iso}\,\breve{\mathbf{T}}_u$. Using (16) and (17) this matrix splits as

$$\breve{\mathbf{B}}_{iso} = \breve{\mathbf{B}}_c + \breve{\mathbf{B}}_h, \quad \text{with} \quad \breve{\mathbf{B}}_c = \breve{\mathbf{T}}_e^{-1}\mathbf{B}_c\breve{\mathbf{T}}_u, \quad \breve{\mathbf{B}}_h = \breve{\mathbf{T}}_e^{-1}(\mathbf{B}_d + \mathbf{B}_\xi\,\xi + \mathbf{B}_\eta\,\eta)\breve{\mathbf{T}}_u. \tag{19}$$

The entries of $\breve{\mathbf{B}}_c$ and $\breve{\mathbf{B}}_h$ are quadratic polynomial functions of ξ and η (*not* rational functions, as is the case for $\mathbf{B}_\xi$ and $\mathbf{B}_\eta$) and of the geometric invariants introduced in Appendix A. For example

$$\breve{\mathbf{B}}_c(1,1) \approx -\frac{L_{21}\big((A_0{-}A_1{+}A_2\eta)(A_0{+}(A_1{+}A_2)\eta\big)}{4A_0A_{412}L_{68}^2}, \quad \breve{\mathbf{B}}_h(3,1) \approx \frac{A_{234}L_{21}\big((A_0{-}A_1)\xi + A_2(\eta{+}2\xi\,\eta)\big)}{2A_0A_{412}L_{75}L_{68}}, \tag{20}$$

in which A_0, A_1 and A_2 are defined in (56). The complete set of entries is not listed to conserve space. For a uniform stress state in which $\mathbf{e}_c = [\, e_{cxx}\ e_{cyy}\ 2e_{cxy}\,]^T = \mathbf{B}_c\mathbf{u}_c$ is constant over the element, the natural strains $\breve{\mathbf{e}}_c = \breve{\mathbf{T}}_e^{-1}\mathbf{e}_c$ are *not* constant unless $A_1 = A_2 = 0$. In fact they are rational functions of ξ and η.

§3.4. Natural Stresses and Constitutive Matrices

The natural stresses energy-conjugate to $\breve{e}_{\xi\xi}$, $\breve{e}_{\eta\eta}$ and $\breve{\gamma}_{\xi\eta}$ will be denoted by $\breve{\sigma}_{\xi\xi}$, $\breve{\sigma}_{\eta\eta}$ and $\breve{\sigma}_{\xi\eta}$, respectively. They are collected in a 3-vector $\breve{\boldsymbol{\sigma}}$, and are linked to their Cartesian counterparts by the transformations $\boldsymbol{\sigma} = \breve{\mathbf{T}}_\sigma\, \breve{\boldsymbol{\sigma}}$ and $\breve{\boldsymbol{\sigma}} = \breve{\mathbf{T}}_\sigma^{-1}\, \boldsymbol{\sigma}$. Let $\mathcal{U} = \frac{1}{2}\mathbf{e}^T\mathbf{E}\,\mathbf{e}$ and $\mathcal{U}^* = \frac{1}{2}\boldsymbol{\sigma}^T\mathbf{C}\,\boldsymbol{\sigma}$ denote the strain and stress energy densities, respectively. ($\mathcal{U}^*$ is also known as the complementary energy density.) Since $\mathbf{e}^T\boldsymbol{\sigma} = \breve{\mathbf{e}}^T\breve{\mathbf{T}}_e^T\,\boldsymbol{\sigma} \stackrel{\text{def}}{=} \breve{\mathbf{e}}^T\breve{\boldsymbol{\sigma}}$ we must have $\breve{\boldsymbol{\sigma}} = \breve{\mathbf{T}}_e^T\,\boldsymbol{\sigma}$ and $\boldsymbol{\sigma} = \breve{\mathbf{T}}_e^{-T}\,\breve{\boldsymbol{\sigma}}$. Consequently the natural stresses are given by the transformations

$$\boldsymbol{\sigma} = \breve{\mathbf{T}}_\sigma\,\breve{\boldsymbol{\sigma}}, \quad \text{with} \quad \breve{\mathbf{T}}_\sigma = \breve{\mathbf{T}}_e^{-T}, \qquad \breve{\boldsymbol{\sigma}} = \breve{\mathbf{T}}_\sigma^{-1}\,\boldsymbol{\sigma}, \quad \text{with} \quad \breve{\mathbf{T}}_\sigma^{-1} = \breve{\mathbf{T}}_e^T. \tag{21}$$

To get the natural versions of the constitutive matrices, note that $2\mathcal{U} = \mathbf{e}^T\,\mathbf{E}\,\mathbf{e} \stackrel{\text{def}}{=} \breve{\mathbf{e}}^T\,\breve{\mathbf{E}}\,\breve{\mathbf{e}}$ and that $2\mathcal{U}^* = \boldsymbol{\sigma}^T\,\mathbf{C}\,\boldsymbol{\sigma} \stackrel{\text{def}}{=} \breve{\boldsymbol{\sigma}}^T\,\breve{\mathbf{C}}\,\breve{\boldsymbol{\sigma}}$. Applying the foregoing strain and stress transformations yields

$$\breve{\mathbf{E}} = \breve{\mathbf{T}}_e^T\,\mathbf{E}\,\breve{\mathbf{T}}_e, \qquad \breve{\mathbf{C}} = \breve{\mathbf{T}}_\sigma^T\,\mathbf{C}\,\breve{\mathbf{T}}_\sigma = \breve{\mathbf{T}}_e^{-1}\,\mathbf{C}\,\breve{\mathbf{T}}_e^{-T}. \tag{22}$$

Check: $\breve{\mathbf{E}}\,\breve{\mathbf{C}} = \breve{\mathbf{T}}_e^T\,\mathbf{E}\,\breve{\mathbf{T}}_e\,\breve{\mathbf{T}}_e^{-1}\,\mathbf{C}\,\breve{\mathbf{T}}_e^{-T} = \breve{\mathbf{T}}_e^T\,\mathbf{E}\,\mathbf{C}\,\breve{\mathbf{T}}_e^{-T} = \breve{\mathbf{T}}_e^T\,\breve{\mathbf{T}}_e^{-T} = \mathbf{I}$. Note that $\breve{\mathbf{E}}$ or $\breve{\mathbf{C}}$ by themselves dont have any direct physical meaning as their Cartesian counterparts do, since they vary with the metric. They are only a convenience tool for element invariant derivations.

§3.5. Natural Equilibrium Equations

For zero body forces the Cartesian differential equilibrium equations are $\mathbf{D}^T\boldsymbol{\sigma} = \mathbf{0}$, which is $(2)_3$ with $\mathbf{b} = \mathbf{0}$. From (15), $\mathbf{D}^T = \breve{\mathbf{T}}_d^{-T}\,\breve{\mathbf{D}}^T\,\breve{\mathbf{T}}_e^T$, and from (21), $\boldsymbol{\sigma} = \breve{\mathbf{T}}_\sigma\,\breve{\boldsymbol{\sigma}} = \breve{\mathbf{T}}_e^{-T}\,\breve{\boldsymbol{\sigma}}$. Replacing gives $\mathbf{D}^T\boldsymbol{\sigma} = \breve{\mathbf{T}}_d^{-T}\,\breve{\mathbf{D}}^T\,\breve{\boldsymbol{\sigma}} = \mathbf{0}$. If $\breve{\mathbf{T}}_d$ is nonsingular, which from (7) is seen to hold as long as $\cos(\phi_1-\phi_2) \neq 0$, it is sufficient to require that $\breve{\mathbf{D}}^T\,\breve{\boldsymbol{\sigma}} = \mathbf{0}$. This expands to the two natural equilibrium equations

$$\frac{1}{J_1}\frac{\bar{\partial}\breve{\sigma}_{\xi\xi}}{\bar{\partial}\xi} + \frac{1}{J_2}\frac{\bar{\partial}\breve{\sigma}_{\xi\eta}}{\bar{\partial}\eta} = 0, \qquad \frac{1}{J_1}\frac{\bar{\partial}\breve{\sigma}_{\xi\eta}}{\bar{\partial}\xi} + \frac{1}{J_2}\frac{\bar{\partial}\breve{\sigma}_{\eta\eta}}{\bar{\partial}\eta} = 0. \tag{23}$$

Equations (23) satisfy differential (pointwise) equilibrium only for elements of constant metric, such as rectangles or parallelograms, since metric coefficients are frozen on taking the $\bar{\partial}$ partials. Differential equations that express pointwise equilibrium for more general geometries are substantially more complicated than (23), but unnecessary in the sequel. Indeed, for developing finite element templates "equilibrium relaxation" is a virtue rather than a blemish.

§3.6. Useful Natural Stress Fields

A natural stress field that satisfies (23) is $\breve{\sigma}_{\xi\xi} = \mu_1\, g_1(\eta)$, $\breve{\sigma}_{\eta\eta} = \mu_2\, g_2(\xi)$, and $\breve{\sigma}_{\xi\eta} = \mu_3$. Here μ_1 through μ_3 are stress-mode amplitudes with physical dimension of stress whereas g_1 and g_2 are arbitrary functions of η and ξ, respectively. In matrix form

$$\begin{bmatrix} \breve{\sigma}_{\xi\xi} \\ \breve{\sigma}_{\eta\eta} \\ \breve{\sigma}_{\xi\eta} \end{bmatrix} = \begin{bmatrix} g_1(\eta) & 0 & 0 \\ 0 & g_2(\xi) & 0 \\ 0 & 0 & 1 \end{bmatrix} \begin{bmatrix} \mu_1 \\ \mu_2 \\ \mu_3 \end{bmatrix}, \quad \text{or} \quad \breve{\boldsymbol{\sigma}} = \breve{\mathbf{A}}\,\boldsymbol{\mu}, \tag{24}$$

For constructing the flexural (higher order) stiffness the following assumption is the simplest one:

$$\begin{bmatrix} \breve{\sigma}_{h\xi\xi} \\ \breve{\sigma}_{h\eta\eta} \\ \breve{\sigma}_{h\xi\eta} \end{bmatrix} = \begin{bmatrix} \eta-\eta_N & 0 \\ 0 & \xi-\xi_N \\ 0 & 0 \end{bmatrix} \begin{bmatrix} \mu_{h1} \\ \mu_{h2} \end{bmatrix}, \quad \text{or} \quad \breve{\boldsymbol{\sigma}}_h = \breve{\mathbf{A}}_h\,\boldsymbol{\mu}_h. \tag{25}$$

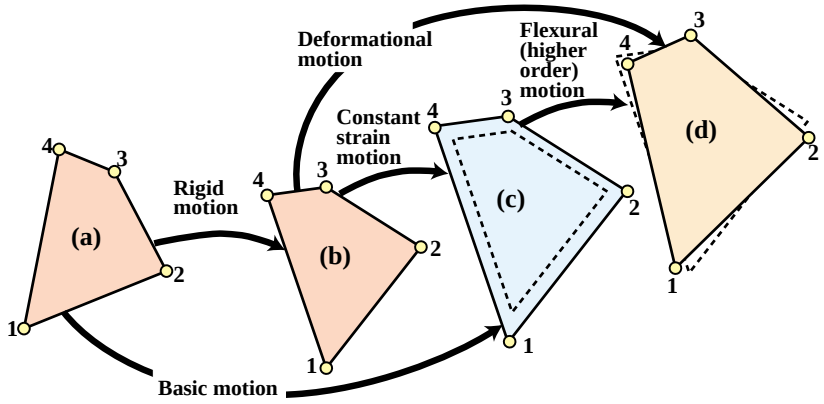

FIGURE 7. Kinematic decomposition of quadrilateral in-plane motion for template development: rigid, constant-strain and flexural (higher order). Several liberties are taken for visualization convenience: (i) motions are actually infinitesimal, (ii) there are no rigid motions from configuration (b) to (c) and from (c) to (d), so in fact the quadrilateral centroid stays in the same location.

In (25) ξ_N and η_N are natural coordinates of lines that may be interpreted as "neutral axes" for bending along the natural directions. If one chooses

$$\xi_N = \xi_C \approx \tfrac{1}{3}A_1/A_0, \qquad \eta_N = \eta_C \approx \tfrac{1}{3}A_2/A_0, \tag{26}$$

where ξ_C, η_C are the centroid coordinates given by (64), the mean values of field (25) over an arbitrary quadrilateral approximately vanish.

§3.7. Kinematic Decomposition

Template development relies on hierarchical divide-and-conquer of the element kinematics. For a 4-node quadrilateral panel, the appropriate two-level decomposition is sketched in Figure 7.

At the top level, the total motion is decomposed into rigid and deformational. The latter is in turn split into constant strain and flexural motions. In the Free Formulation [8–11,14,15,46,55], the notation for the three components is shortened to r-motion, c-motion and h-motion, where h stands for "higher order" behavior. Those labels will be often used as subscripts in the ensuing material. The combination of rigid and constant strain is collectively called the basic motion, and subscripted by either rc or b.

The total motion of element e is defined by the total node displacements $\mathbf{u}^e$. The appropriate decomposition is $\mathbf{u}^e = \mathbf{u}^e_r + \mathbf{u}^e_c + \mathbf{u}^e_h$. But this is not particularly useful because it conceals the physics. It is better to describe each portion in terms of generalized coordinates $\mathbf{q}_r$, $\mathbf{q}_c$ and $\mathbf{q}_h$, respectively, which are grouped in a vector $\mathbf{q}$. To each generalized coordinate is associated a kinematic field called a *mode* for brevity. Thus we speak of r-modes, c-modes and h-modes. Using the Free Formulation notation we write

$$\mathbf{u}^e = \mathbf{G}_r\,\mathbf{q}_r + \mathbf{G}_c\,\mathbf{q}_c + \mathbf{G}_h\,\mathbf{q}_h = [\,\mathbf{G}_r\;\;\mathbf{G}_c\;\;\mathbf{G}_h\,]\begin{bmatrix}\mathbf{q}_r\\ \mathbf{q}_c\\ \mathbf{q}_h\end{bmatrix} = \mathbf{G}\,\mathbf{q}. \tag{27}$$

For the quadrilateral panel the dimensions of $\mathbf{q}_r$, $\mathbf{q}_c$ and $\mathbf{q}_h$ are 3, 3 and 2, respectively. Hence the dimension of $\mathbf{G}_r$, $\mathbf{G}_c$, $\mathbf{G}_h$ and $\mathbf{G}$ are 8×3, 8×3, 8×2 and 8×8, respectively. Notice that the choice of $\mathbf{q}_r$, $\mathbf{q}_c$ and $\mathbf{q}_h$ is left open as a matter of convenience. The obvious picks for $\mathbf{q}_r$ and $\mathbf{q}_c$ are the 3 rigid-body mode amplitudes and the 3 constant-strain mode amplitudes, respectively. But for $\mathbf{q}_h$ the choice is far from obvious if the element has arbitrary geometry. In-plane flexural motions are

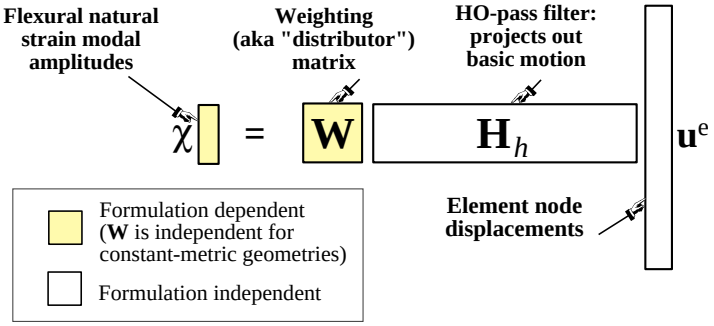

FIGURE 8. The anatomy of higher-order natural strain extraction for the quadrilateral panel: multiplicative decomposition into a 2×2 weighting matrix $\mathbf{W}$ and a 2×8 h-mode pass filter (basic-motion-kill projector) $\mathbf{H}_h$.

attractive candidates, but how should they be defined? Several choices have been explored over the past two decades.

In the Free Formulation, all modes: r, c and h, are *explicitly defined as displacement fields*. Matrix $\mathbf{G}$ is built by evaluation of these fields at nodes, inverted producing $\mathbf{H} = \mathbf{G}^{-1}$, and row-wise partitioned to yield

$$\mathbf{q} = \begin{bmatrix} \mathbf{q}_r \\ \mathbf{q}_c \\ \mathbf{q}_h \end{bmatrix} = \mathbf{H}\,\mathbf{u}^e = \begin{bmatrix} \mathbf{H}_r \\ \mathbf{H}_c \\ \mathbf{H}_h \end{bmatrix} \mathbf{u}^e. \tag{28}$$

For the quadrilateral panel $\mathbf{H}_r$, $\mathbf{H}_c$ and $\mathbf{H}_h$ are 3×8, 3×8 and 2×8 matrices, respectively. Once (28) is available, the construction of the stiffness matrix is routine.

In the ANDES formulation [16,26,44], the h-field is constructed indirectly by assuming deviatoric strain patterns. That is, deviations from constant strain states. No attempt is made at constructing a higher order displacement field. This would be generally impossible because assumed deviatoric strain fields are not necessarily compatible, and thus not integrable. This relaxation provides additional freedom to element developers.

In the template approach the operational flexibility is taken to the limit. The higher order component is constructed as a parametrized algebraic expression. As a result, a template can generate all elements that fit the decomposition of Figure 7. In particular it embodies Free Formulation and ANDES elements as instances, as well as those produced by other techniques.

§3.8. Kinematic Filters

A Free Formulation tool that survives in the wider context of templates is the concept of *filter matrices*. To state the problem, consider (28). Given $\mathbf{u}^e$, the job of matrices $\mathbf{H}_r$, $\mathbf{H}_c$ and $\mathbf{H}_h$ is to extract the generalized coordinate amplitudes: $\mathbf{q}_r = \mathbf{H}_r\mathbf{u}^e$, $\mathbf{q}_c = \mathbf{H}_c\mathbf{u}^e$ and $\mathbf{q}_h = \mathbf{H}_h\mathbf{u}^e$. This is a *kinematic filtering* process, hence the name. For an element of given node and freedom configuration, the construction of $\mathbf{H}_r$ and $\mathbf{H}_c$ is the *same for all possible element instances*, as long as the formulation exactly reproduces rigid body modes and constant strain states. And so it may be done once and for all: $\mathbf{H}_r$ and $\mathbf{H}_c$ will be the same today, tomorrow or as long as the Universe endures.

The filter matrix $\mathbf{H}_h$ is another matter entirely. It is formulation dependent and can vary from instance to instance. With a view to unifying all such possibilities into one template, it is convenient to effect a *multiplicative decomposition* of $\mathbf{H}_h$ into a formulation-dependent weighting matrix (also called a "h-mode distributor") and a formulation-independent filter matrix that weeds out basic modes. The name $\mathbf{H}_h$ will be reserved for the latter. This decomposition is pictured in Figure 8.

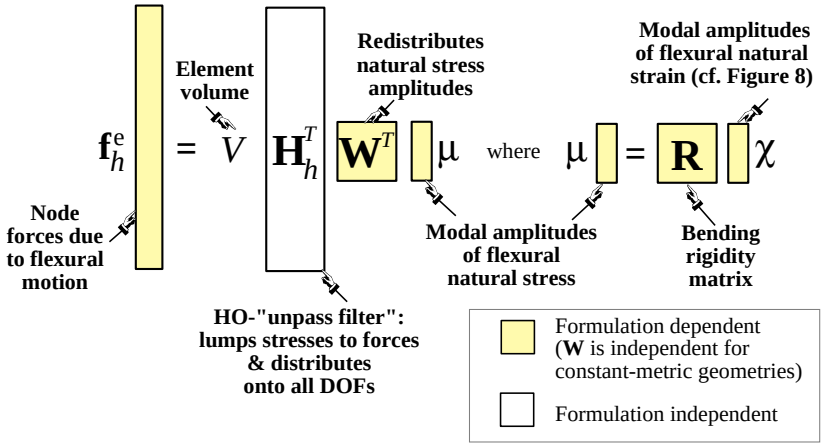

FIGURE 9. Roadmap from flexural natural strains, through natural stresses, ending in node forces: continuation of Figure 8.

The derivation of $\mathbf{H}_h$ and $\mathbf{W}$ for a quadrilateral panel of arbitrary geometry was carried out using a variational *strain fitting* method described in [25]. This procedure requires extensive use of the invariant relations presented in Appendix A as well as the higher order natural strain-displacement matrix $\breve{\mathbf{B}}_h$ defined in (19). The long symbolic computations were done with *Mathematica*. Details are omitted to save space. The higher-order pass filter matrix turned out to be

$$\mathbf{H}_h = \begin{bmatrix} H_1 & 0 & H_2 & 0 & H_3 & 0 & H_4 & 0 \\ 0 & H_1 & 0 & H_2 & 0 & H_3 & 0 & H_4 \end{bmatrix}, \tag{29}$$

where H_i are the dimensionless area-ratios defined in (65). This matrix is the same for all elements of this type. Matrix $\mathbf{W}$ depends on assumptions made on (generally incompatible) natural flexural strain variations. These are energy fitted to the compatible strains defined by $\breve{\mathbf{B}}_h$. For the simplest assumption of linear variation in ξ and η a surprisingly simple closed form emerges. Introducing the abbreviations $x_{12|34} = (x_{12}+x_{34})/2$, $y_{12|34} = (y_{12}+y_{34})/2$, $x_{21|34} = (x_{21}+x_{34})/2$, $y_{21|34} = (y_{21}+y_{34})/2$, $x_{32|41} = (x_{32}+x_{41})/2$ and $y_{32|41} = (y_{32}+y_{41})/2$, and denoting the lengths of the quadrilateral medians 5–7 and 6–8 shown in Figure 16(b) by L_{68} and L_{57}, respectively, one finds

$$\mathbf{W} = \begin{bmatrix} \dfrac{x_{21|34} + \Upsilon_\xi x_{12|34}}{L_{68}^2} & \dfrac{y_{21|34} + \Upsilon_\xi y_{12|34}}{L_{68}^2} \\ \dfrac{x_{32|41} + \Upsilon_\eta x_{12|34}}{L_{75}^2} & \dfrac{y_{32|41} + \Upsilon_\eta y_{12|34}}{L_{75}^2} \end{bmatrix}. \tag{30}$$

Here Υ_ξ and Υ_η are dimensioness coefficients characterizing the location of "neutral flexure axes" over the element. These vanish if $A_1 = A_2 = 0$. Other fitted-strain distributions would lead to different $\mathbf{W}$ entries. All of them, however, can be expressed in the universal form

$$\mathbf{W} = \begin{bmatrix} \dfrac{x_{W68}}{L_{68}^2} & \dfrac{y_{W68}}{L_{68}^2} \\ \dfrac{x_{W75}}{L_{75}^2} & \dfrac{y_{W75}}{L_{75}^2} \end{bmatrix}, \tag{31}$$

in which the numerators have dimensions of length. Their algebraic structure can be left free as part of the template. One constraint, however, ought to be respected: if the element has constant metric so that $A_1 = A_2 = 0$ (rectangle or parallellogram), $x_{W68} = x_{68}$, $y_{W68} = y_{68}$, $x_{W75} = x_{75}$ and $y_{W75} = y_{75}$.

§3.9. Flexural Rigidity

The matrix operation $\boldsymbol{\chi} = \mathbf{W}\,\mathbf{H}_h\,\mathbf{u}^e$ depicted in Figure 8 extracts two flexural-mode natural strain amplitudes: χ_1 and χ_2. These are dimensionless. The corresponding amplitudes of flexural natural stresses are μ_1 and μ_2, which have physical dimension of stress. The 2-vectors $\boldsymbol{\chi}$ and $\boldsymbol{\mu}$ are connected by the 2×2 *flexural rigidity matrix* $\mathbf{R}$. This matrix brings up the higher order constitutive behavior:

$$\boldsymbol{\mu} = \begin{bmatrix} \mu_1 \\ \mu_2 \end{bmatrix} = \begin{bmatrix} R_{11} & R_{12} \\ R_{12} & R_{22} \end{bmatrix} \begin{bmatrix} \chi_1 \\ \chi_2 \end{bmatrix} = \mathbf{R}\,\boldsymbol{\chi}, \tag{32}$$

Entries of $\mathbf{R}$ have dimension of stress. They can be conveniently expressed from entries of the natural elasticity matrix $\breve{\mathbf{E}}$, or of the natural compliance matrix $\breve{\mathbf{C}}$. These in turn can be written in terms of the more accessible Cartesian elasticity or compliance matrix, respectively, using the inverses of (22).

How is $\mathbf{R}$ calculated? Outside the template context this would depend on the formulation. In well established displacement- and strain-assumed methods, (e.g, shape functions, reduced integration, Free Formulation, ANS or ANDES), $\mathbf{R}$ is built as a generalized bending rigidity matrix. In stress-assumed hybrids, Trefftz or HR-based formulations $\mathbf{R}$ emerges as the inverse of a generalized bending flexibility. In any event $\mathbf{R}$ is a consequence of the chosen method and cannot be played with.

In the template approach, however, $\mathbf{R}$ is left unspecified as part of the template. This freedom of choice may be used to either fit existing elements, or to produced new customized elements.

§3.10. Flexural Node Forces

The final step in dealing with the flexural motion is to arrive to the flexural nodal forces $\mathbf{f}_h$. From virtual work, this is done simply by premultiplying $\boldsymbol{\mu}$ by $\mathbf{W}^T$ and $\mathbf{H}_h^T$, in that order, and scaling through by the element volume $V = Ah$ to restore the correct physical units:

$$\mathbf{f}_h = V\,\mathbf{H}_h^T\,\mathbf{W}^T\,\boldsymbol{\mu} = V\,\mathbf{H}_h^T\,\mathbf{W}^T\,\mathbf{R}\,\mathbf{W}\,\mathbf{H}_h\,\mathbf{u}^e = \mathbf{K}_h\,\mathbf{u}^e \tag{33}$$

Here $\mathbf{K}_h = V\,\mathbf{H}_h^T\,\mathbf{W}^T\,\mathbf{R}\,\mathbf{W}\,\mathbf{H}_h$ is the higher order stiffness matrix, which for this element is entirely due to in-plane flexural motions. The sequence is depicted in Figure 9, which completes Figure 8.

§4. Templates

After the preparatory work of Section 3, we are ready to present the template for the quadrilateral panel. All 4-node quadrilateral stiffness matrices that pass the IET (individual element patch-test) of Bergan and Hanssen [7,29] are instances of the algebraic form

$$\mathbf{K} = \mathbf{K}_b + \mathbf{K}_h = V\,\mathbf{H}_c^T\mathbf{E}\mathbf{H}_c + V\,\mathbf{H}_h^T\,\mathbf{W}^T\,\mathbf{R}\,\mathbf{W}\,\mathbf{H}_h, \tag{34}$$

where most symbols have been previously defined. For the convenience of the reader the ingredients are restated:

$$\begin{aligned}
\mathbf{H}_c &= \frac{1}{2A}\begin{bmatrix} y_{24} & 0 & y_{31} & 0 & y_{42} & 0 & y_{13} & 0 \\ 0 & x_{42} & 0 & x_{13} & 0 & x_{24} & 0 & x_{31} \\ x_{42} & y_{24} & x_{13} & y_{31} & x_{24} & y_{42} & x_{31} & y_{13} \end{bmatrix}, \\
\mathbf{H}_h &= \begin{bmatrix} H_1 & 0 & H_2 & 0 & H_3 & 0 & H_4 & 0 \\ 0 & H_1 & 0 & H_2 & 0 & H_3 & 0 & H_4 \end{bmatrix}, \\
\mathbf{W} &= \begin{bmatrix} W_{11} & W_{12} \\ W_{21} & W_{22} \end{bmatrix}, \quad \mathbf{R} = \begin{bmatrix} R_{11} & R_{12} \\ R_{12} & R_{22} \end{bmatrix}, \quad V = Ah.
\end{aligned} \tag{35}$$

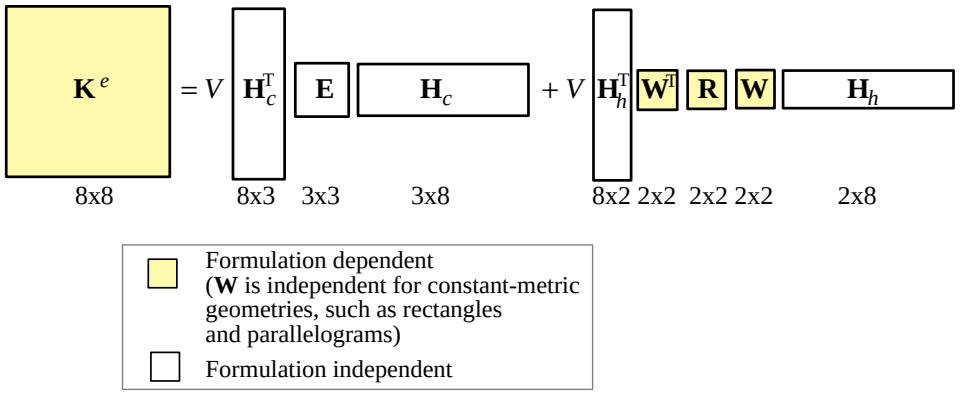

FIGURE 10. The template for the 4-node quadrilateral panel, highlighting formulation dependent and independent parts.

$\mathbf{H}_c$ and $\mathbf{H}_h$ are the same for all quadrilateral models. Note that $\mathbf{H}_c$, the constant-strain pass filter, agrees with the mean isoparametric strain-displacement matrix $\mathbf{B}_c$ in (17). This is not an accident. The coalescence holds for any element in which constant strain implies constant stress [19]. This is the case here because the element is assumed to have uniform thickness and constitutive properties.

Both $\mathbf{R}$ and $\mathbf{W}$ are formulation dependent. For constant metric shapes, namely rectangles and parallelograms, $\mathbf{W}$ is diagonal and formulation independent [27]. The important point is that the element derivation affects only part of the stiffness expression, as highlighted in Figure 10.

§4.1. Template Terminology

The algebraic form characterized by (34) and (35) is called a finite element stiffness template, or *template* for short. Matrices $\mathbf{K}_b$ and $\mathbf{K}_h$ are called the basic and higher-order stiffness matrix, respectively, in accordance with the fundamental decomposition of the Free Formulation. These two matrices play different and complementary roles. The basic stiffness $\mathbf{K}_b$ takes care of consistency and element-type-mixing. In the Free Formulation a restatement of the basic stiffness (34) is preferred:

$$\mathbf{K}_b = V^{-1}\,\mathbf{L}\,\mathbf{E}\,\mathbf{L}^T, \tag{36}$$

where $\mathbf{L}$ is called the force lumping matrix, or simply lumping matrix. If the element has uniform thickness and material properties, $\mathbf{L} = \mathbf{H}_c/V$.

The higher order stiffness $\mathbf{K}_h$ is a *stabilization* term that provides the correct rank and may be adjusted for accuracy. This matrix is orthogonal to rigid body motions and constant strain states. To verify the claim for this template introduce the basic-mode matrix $\mathbf{G}_{rc}$ of the Free Formulation, which merges $\mathbf{G}_r$ and $\mathbf{G}_c$ of (27) column-wise:

$$\mathbf{G}_{rc} = \begin{bmatrix} 1 & 0 & y_1 & x_1 & 0 & y_1 \\ 0 & 1 & -x_1 & 0 & y_1 & x_1 \\ 1 & 0 & y_2 & x_2 & 0 & y_2 \\ 0 & 1 & -x_2 & 0 & y_2 & x_2 \\ 1 & 0 & y_3 & x_3 & 0 & y_3 \\ 0 & 1 & -x_3 & 0 & y_3 & x_3 \\ 1 & 0 & y_4 & x_4 & 0 & y_4 \\ 0 & 1 & -x_4 & 0 & y_4 & x_4 \end{bmatrix} \tag{37}$$

Columns of $\mathbf{G}_{rc}$ span node-evaluated rigid body modes and constant strain states. These are not orthonormalized as that property is not required here. It is readily checked that $\mathbf{H}_h\mathbf{G}_{rc} = \mathbf{0}$. Hence those

modes, and any linear combination thereof, are orthogonal to the higher order stiffness: $\mathbf{K}_h\mathbf{G}_{rc} = \mathbf{0}$ for any $\mathbf{W}$ and $\mathbf{R}$. The role of $\mathbf{H}_h$ as a "higher-order pass filter" displayed in Figure 8 is confirmed.

§4.2. Requirements

An acceptable template fulfills four conditions: (C) consistency, (S) stability (correct rank), (I) observer invariance and (P) parametrization. These are discussed at length in other papers [18–24]. Conditions (C) and (S) are imposed to ensure convergence as the mesh size is reduced by enforcing *a priori* satisfaction of the Individual Element Test. Observer invariance has to be checked by rotating the $\{x, y\}$ axes and verifying that both $\mathbf{K}_b$ and $\mathbf{K}_h$ transform correctly. Condition (P) means that the template contains free parameters or free matrix entries. In the present template the simplest choice of parameters are the matrix entries of $\mathbf{R}$ and $\mathbf{W}$. As these always appear in the combination $\mathbf{W}^T\mathbf{R}\mathbf{W}$, some indeterminacy arises because adjustments in $\mathbf{W}$ can be moved to $\mathbf{R}$ or vice-versa. To fulfill stability, $R_{11} > 0$, $R_{22} > 0$ and $R_{11}R_{22} - R_{12}^2 > 0$. Parametrization facilitates performance optimization as well as tuning elements, or combinations of elements, to fulfill specific needs.

Using the IET as departure point it is not difficult to show [45] that the given template, under the stated restrictions on $\mathbf{R}$, includes all elements of this type that satisfy the IET and stability.

§4.3. Instances, Signatures, Clones

Setting free parameters to specific values yields element instances. This set is called the template *signature*, a term introduced in 1999 [22,23]. Borrowing terminology from biogenetics, the signature may be viewed as an "element DNA" that uniquely characterizes it as an individual entity. Elements derived by different techniques that share the same signature are called *clones*, except for the first born.

One of the "template services" is automatic identification of clones. If two elements fitting the template (34)–(35) share $\mathbf{R}$ and $\mathbf{W}$, they are clones. Inasmuch as most FEM formulation schemes have been tried on this element, it should come as no surprise that there are many clones, particularly for the rectangular shape specialization discussed next.

§5. Specialization 1: The Rectangular Panel

A template such as (34)–(35) may be on first sight disconcerting to the reader. This is not the usual way in which elements are presented in FEM textbooks. The dominant tradition is to develop individual elements in total (non-decomposed) form using specific methods. More about this practice is said in the Conclusions section.

The specialization of the general template to a rectangular panel, often abbreviated to RP in the sequel, has been effectively used by the writer as a tutorial device in graduate level FEM courses. This geometry is simple enough to be amenable to complete analytical development, even for anisotropic material behavior, but it possesses a nontrivial template.

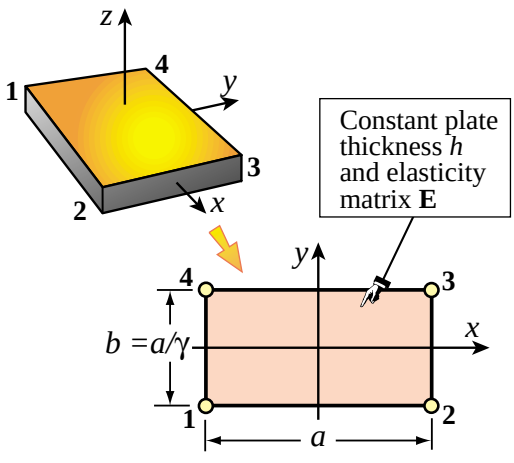

FIGURE 11. The rectangular panel.

In addition, the rectangular panel serves as a convenient vehicle to teach the phenomenon of shear locking and explain the use of reduced integration within a template perspective. The material in this and the next section is extracted from course notes as well as from a recent expository article [27].

Table 2. A Clone Gallery for the Rectangular Panel

Name	Description	Clones and sources
StressRP	5-stress-mode element	Direct derivation: Turner et al [61], Gallagher [28] Pian 5-mode stress hybrid [50,49,53] Wilson-Taylor-Doherty-Ghaboussi Q6 [62] Taylor-Wilson-Beresford QM6 [60] Belytschko-Liu-Engelmann QBI [6] SRI of iso-P model with elasticity split (50).
StrainRP	5-strain-mode element	MacNeal QUAD4 [40,38] SRI of iso-P model with elasticity split (52).
DispRP	Bilinear iso-P element	Argyris [3] as edge stiffened rectangular panel Taig-Kerr [59] as specialization of quadrilateral

Note 1: Many plane stress models listed above were derived for quadrilateral geometries, and a few as membrane component of shells. The right-hand-column classification only pertains to the rectangular panel specialization. For example, Q6 and QM6 differ for variable-metric shapes.

Note 2: Instances of the extra-stress-mode-hybrids and displacement-bubble-function "futile families" are covered in [27]

Note 3: Post-1990 clones (e.g. EAS [54]) omitted to save space. See Lautersztajn and Samuelsson [37] for a recent survey.

§5.1. Stiffness Template

The rectangular panel is depicted in Figure 11. The $\{x, y\}$ axes are aligned with the sides for conveniency. The in-plane dimensions are a and $b = a/\gamma$, where $\gamma = a/b$ is the side aspect ratio. The thickness h and elasticity matrix $\mathbf{E}$ are constant over the element. For this geometry,

$$
\begin{aligned}
\mathbf{H}_c &= \frac{1}{2ab}\begin{bmatrix} -b & 0 & b & 0 & b & 0 & -b & 0 \\ 0 & -a & 0 & -a & 0 & a & 0 & a \\ -a & -b & -a & b & a & b & a & -b \end{bmatrix}, \\
\mathbf{H}_h &= \tfrac{1}{2}\begin{bmatrix} 1 & 0 & -1 & 0 & 1 & 0 & -1 & 0 \\ 0 & 1 & 0 & -1 & 0 & 1 & 0 & -1 \end{bmatrix}, \\
\mathbf{W} &= \begin{bmatrix} 1/a & 0 \\ 0 & 1/b \end{bmatrix}, \quad \mathbf{R} = \begin{bmatrix} R_{11} & R_{12} \\ R_{12} & R_{22} \end{bmatrix}, \quad V = abh.
\end{aligned}
\tag{38}
$$

The only freedom left in the template is the choice of R_{11}, R_{22} and R_{12}. Three prototypical instances that serves as guide in this choice are

- The stress-assumed model StressRP.
- The strain-assumed model StrainRP.
- The displacement-assumed bilinear isoparametric model DispRP.

The derivation of StressRP and StrainRP is covered in detail in the tutorial [27], whereas that of DispRP

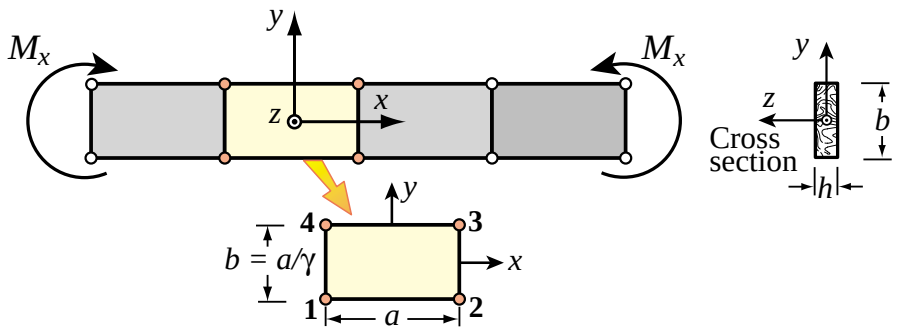

FIGURE 12. The in-plane constant-moment bending test along the x direction.

is standard textbook material. For these models $\mathbf{R}$ becomes $\mathbf{R}_\sigma$, $\mathbf{R}_e$ and $\mathbf{R}_u$, respectively, where

$$\mathbf{R}_\sigma = \tfrac{1}{3}\begin{bmatrix} C_{11}^{-1} & 0 \\ 0 & C_{22}^{-1} \end{bmatrix}, \quad \mathbf{R}_e = \tfrac{1}{3}\begin{bmatrix} E_{11} & 0 \\ 0 & E_{22} \end{bmatrix}, \quad \mathbf{R}_u = \tfrac{1}{3}\begin{bmatrix} E_{11} + \dfrac{a^2 E_{33}}{b^2} & \dfrac{bE_{13}}{a} + \dfrac{aE_{23}}{b} \\ \dfrac{bE_{13}}{a} + \dfrac{aE_{23}}{b} & E_{22} + \dfrac{b^2 E_{33}}{a^2} \end{bmatrix} \tag{39}$$

As narrated in Section 7, beginning in the mid-1950s most FEM formulation methods have been tried on the rectangular panel, as well as its plane strain and axisymmetric counterparts. Thus it should be no surprise that after five decades many clones exist, particularly of the stress element. Those published before 1990 are collected in Table 2. For example, the incompatible mode element Q6 of Wilson et al [62] is a clone of StressRP. The version QM6 of Taylor et al [60], which passes the patch test for arbitrary shape, reduces to Q6 for rectangles and parallelograms. Even for this exceedingly simple geometry, recognition of some of the coalescences took some time, as recently recollected by Pian [53].

§5.2. Finding the Best

The obvious question arises: among the infinity of elements that a template such as (38) can generate, is there a best one? By construction all instances verify exactly the IET for rigid body modes and uniform strain states. Hence the optimality criterion must rely on higher order patch tests. The obvious tests involve response to in-plane bending along the side directions. This leads to comparisons in the form of energy ratios. These have been used since 1984 to tune up the higher order stiffness of triangular elements [10,14,16,26]. An extension introduced here is consideration of arbitrary anisotropic material.

The x bending test is depicted in Figure 12. A Bernoulli-Euler plane beam of thin rectangular cross-section with height b and thickness h (normal to the plane of the figure) is bent under applied end moments M_x. The beam is fabricated of anisotropic material with the elasticity matrix $(1)_2$. The exact solution of the beam problem (from both the theory-of-elasticity and beam-theory standpoints) is a constant bending moment $M(x) = M_x$ along the span. The associated stress field is $\sigma_{xx} = -M_x\, y/I_b$, $\sigma_{yy} = \sigma_{xy} = 0$, where $I_b = hb^3/12$, and the energy taken over a length a is $U_x^{\text{beam}} = 6aC_{11}M_x^2/b^3h$. For the 2D element tests, each beam is modeled with one layer of identical 4-node rectangular panels of aspect ratio $\gamma = a/b$. By analogy with the exact solution, all rectangles in the finite element model will undergo the same deformations and stresses. We can therefore consider a typical element as shown in the figure. A simple calculation shows that the element node displacement vector is

$$\mathbf{u}_{bx} = \frac{12M_xC_{11}a}{b^2h}\,[\,-1 \quad 0 \quad 1 \quad 0 \quad -1 \quad 0 \quad 1 \quad 0\,]^T \tag{40}$$

and that the energy taken by the element is $U_x^{\rm panel} = \frac{1}{2}\mathbf{u}_{bx}^T\mathbf{K}\mathbf{u}_{bx}$. The *energy ratio* is defined by $r_x = U_x^{\rm panel}/U_x^{\rm beam}$. This happens to be the ratio of the exact (beam) displacement solution to that of the rectangular panel solution. Hence $r_x = 1$ means that we get the exact answer under M_x, that is, the panel is x-bending exact. If $r_x > 1$ or $r_x < 1$ the panel is overstiff or overflexible in x bending, respectively. A completely analogous test can be set up for y bending, by stacking elements along that direction, and the corresponding energy ratio is called r_y.

§5.3. The Optimal Panel

If $r_x = 1$ and $r_y = 1$ for any aspect ratio $\gamma = a/b$ and arbitrary material properties the element is called *bending optimal*. If $r_x >> 1$ for $a >> b$ and/or $r_y >> 1$ for $a << b$ the element is said to experience *aspect ratio locking* along the x or y direction, respectively. This is called *shear locking* in the FEM literature because it is traceable to spurious shear energy, as shown below.

Applying the tests to the rectangular panel template yields $r_x = 3C_{11}R_{11}$ and $r_y = 3C_{22}R_{22}$. Clearly to get $r_x = r_y = 1$ for any aspect ratio we must take

$$R_{11} = \tfrac{1}{3}C_{11}^{-1}, \quad R_{22} = \tfrac{1}{3}C_{22}^{-1} \tag{41}$$

Since R_{12} is absent from (41) one can set $R_{12} = 0$ for convenience. Comparing to the list (39) shows that StressRP (and clones) *is the bending-optimal rectangular panel*. For isotropic material $R_{11} = R_{22} = E/3$.

§5.4. The Strain Element Does Not Lock

It is interesting to apply the foregoing test to other template instances. The StrainRP element generated by the $\mathbf{R}_e$ of (39) gives

$$r_x = C_{11}E_{11}, \qquad r_y = C_{22}E_{22}. \tag{42}$$

If the material is isotropic, $C_{11} = C_{22} = 1/E$ and $E_{11} = E_{22} = E/(1-\nu^2)$. This yields $r_x = r_y = 1/(1-\nu^2)$, which varies between 1 and 4/3 for Poisson's ratio in the range [0,1/2]. For an orthotropic body with principal material axes aligned with the rectangle sides, $E_{11} = E_1/(1-\nu_{12}\nu_{21})$, $E_{22} = E_2/(1-\nu_{12}\nu_{21})$, $C_{11} = 1/E_1$, $C_{22} = 1/E_2$, and $r_x = r_y = 1/(1-\nu_{12}\nu_{21})$. These are independent of the aspect ratio γ. Consequently StrainRP and its clones *do not lock*, although the element is not generally optimal. Note that if $C_{11}E_{11}$ and/or $C_{22}E_{22}$ differ widely from 1, as may happen in highly anisotropic materials, the bending performance will be poor. The benchmark example of Section 5.9 displays this effect vividly.

§5.5. But the Displacement Element Does

Instance DispRP is generated by the $\mathbf{R}_u$ in (39). Inserting this into the energy ratio yields

$$\begin{aligned} r_x &= C_{11}(E_{11} + E_{33}\gamma^2) = \frac{(E_{22}E_{33} - E_{23}^2)(E_{11} + E_{33}\gamma^2)}{\det(\mathbf{E})}, \\ r_y &= C_{22}(E_{22} + E_{33}\gamma^{-2}) = \frac{(E_{11}E_{33} - E_{13}^2)(E_{22} + E_{33}\gamma^{-2})}{\det(\mathbf{E})}. \end{aligned} \tag{43}$$

in which $\det(\mathbf{E}) = E_{11}E_{22}E_{33} + 2E_{12}E_{13}E_{23} - E_{11}E_{23}^2 - E_{22}E_{13}^2 - E_{33}E_{12}^2$. For an isotropic material

$$r_x = \frac{2 + \gamma^2(1-\nu)}{2(1-\nu^2)}, \qquad r_y = \frac{1 + 2\gamma^2 - \nu}{2\gamma^2(1-\nu^2)}. \tag{44}$$

These relations clearly indicate aspect ratio locking for bending along the longest side dimension. For instance if $\nu = 0$ and $a = 10\,b$, whence $\gamma = a/b = 10$, then $r_x = 51$ and DispRP is over 50 times stiffer in x bending than the Bernoulli-Euler beam element. Expressions (43) make clear that *locking happens for any material law* as long as $E_{33} \neq 0$. Since this is the shear modulus, the name *shear locking* used in the FEM literature is justified.

§5.6. Multiple Element Layers

Results of the energy bending test can be readily extended to predict the behavior of $2n$ ($n = 1, 2, \ldots$) identical layers of elements symmetrically placed through the beam height. If $2n$ layers are placed along the y direction in the configuration of Figure 12 and γ is kept fixed, the energy ratio becomes

$$r_x^{(2n)} = \frac{2^{2n} - 1 + r_x}{2^{2n}}, \tag{45}$$

where r_x is the ratio for one layer. If $r_x \equiv 1$ then $r_x^{2n} \equiv 1$ so bending exactness is maintained, as can be expected. For example, if $n = 1$ (two element layers), $r_x^{(2)} = (3 + r_x)/4$.

§5.7. SRI in Template Context

It is illuminating to study a well known "shear unlocking" device from the standpoint of templates. Full Reduced Integration (FRI) and Selective Reduced Integration (SRI) emerged during 1969–72 [13,36,48,64] as tools to improve the in-plane bending behavior of isoparametric displacement models. Initially labeled as "variational crimes" by Strang [56,57] they were eventually justified through lawful association with mixed variational methods [30–33]. They turned out to be particularly useful for legacy and nonlinear FEM codes because they allow shape function and numerical integration modules to be reused. For the 4-node rectangular panel only SRI is of interest because FRI leads to rank deficiency: $R_{11} = R_{12} = R_{22} = 0$. An interesting question is: can a given template (in particular, StressRP) be reproduced for *any material law* by a SRI scheme? It will be shown that the answer is yes if $R_{12} = 0$. Split the plane stress elasticity matrix $\mathbf{E}$ into $\mathbf{E} = \mathbf{E}_{\rm I} + \mathbf{E}_{\rm II}$. A general parametrization of this splitting that retains symmetry is

$$\mathbf{E} = \mathbf{E}_{\rm I} + \mathbf{E}_{\rm II} = \begin{bmatrix} E_{11}\,\rho_1 & E_{12}\rho_3 & E_{13}\tau_2 \\ E_{12}\,\rho_3 & E_{22}\,\rho_2 & E_{23}\tau_2 \\ E_{13}\,\tau_2 & E_{23}\,\tau_2 & E_{33}\tau_1 \end{bmatrix} + \begin{bmatrix} E_{11}(1-\rho_1) & E_{12}(1-\rho_3) & E_{13}(1-\tau_2) \\ E_{12}(1-\rho_3) & E_{22}(1-\rho_2) & E_{23}(1-\tau_3) \\ E_{13}(1-\tau_2) & E_{23}(1-\tau_3) & E_{33}(1-\tau_1) \end{bmatrix}, \tag{46}$$

in which ρ_1, ρ_2, ρ_3, τ_1, τ_2 and τ_3 are dimensionless coefficients to be chosen. To apply SRI to the isoparametric bilinear model, insert (46) into $\mathbf{E}$ of that formulation to get

$$\mathbf{K} = \int_{\Omega^e} h\,\mathbf{B}_{iso}^T\mathbf{E}_{\rm I}\,\mathbf{B}_{iso}\,d\Omega + \int_{\Omega^e} h\,\mathbf{B}_{iso}^T\mathbf{E}_{\rm II}\,\mathbf{B}_{iso}\,d\Omega = \mathbf{K}_{\rm I} + \mathbf{K}_{\rm II}. \tag{47}$$

where $\mathbf{B}_{iso}$ is given by (16). The two matrices in (47) are computed through different numerical quadrature schemes, labeled (I) and (II). For this element (I) and (II) will be the 1×1 (one point) and 2×2 (4-point) Gauss product rules, respectively. Carrying out the symbolic calculations and comparing to (38) shows that a template with $R_{12} = 0$ and arbitrary $\{R_{11}, R_{22}\}$ can be matched by taking

$$\rho_1 = \frac{1 - 3R_{11}}{E_{11}}, \quad \rho_2 = \frac{1 - 3R_{22}}{E_{22}}, \quad \tau_1 = \tau_2 = \tau_3 = 1. \tag{48}$$

Since ρ_3 does not appear, it is convenient to set $\rho_3 = 1$ to get a diagonal $\mathbf{E}_{\rm II}$. The resulting split is

$$\mathbf{E}_{\rm I} + \mathbf{E}_{\rm II} = \begin{bmatrix} E_{11} - 3R_{11} & E_{12} & E_{13} \\ E_{12} & E_{22} - 3R_{22} & E_{23} \\ E_{13} & E_{23} & E_{33} \end{bmatrix} + \begin{bmatrix} 3R_{11} & 0 & 0 \\ 0 & 3R_{22} & 0 \\ 0 & 0 & 0 \end{bmatrix}, \tag{49}$$

To get the optimal element (StressRP) set $R_{11} = \frac{1}{3}C_{11}^{-1}$ and $R_{22} = \frac{1}{3}C_{22}^{-1}$:

$$\mathbf{E}_{\rm I} + \mathbf{E}_{\rm II} = \begin{bmatrix} E_{11} - C_{11}^{-1} & E_{12} & E_{13} \\ E_{12} & E_{22} - C_{22}^{-1} & E_{23} \\ E_{13} & E_{23} & E_{33} \end{bmatrix} + \begin{bmatrix} C_{11}^{-1} & 0 & 0 \\ 0 & C_{22}^{-1} & 0 \\ 0 & 0 & 0 \end{bmatrix}, \tag{50}$$

For isotropic material this becomes

$$\mathbf{E}_{\rm I} + \mathbf{E}_{\rm II} = \frac{E}{1-\nu^2} \begin{bmatrix} \nu^2 & \nu & 0 \\ \nu & \nu^2 & 0 \\ 0 & 0 & \frac{1}{2}(1-\nu) \end{bmatrix} + E \begin{bmatrix} 1 & 0 & 0 \\ 0 & 1 & 0 \\ 0 & 0 & 0 \end{bmatrix}. \tag{51}$$

To match the (suboptimal) StrainRP, in which $R_{11} = \frac{1}{3}E_{11}$ and $R_{22} = \frac{1}{3}E_{22}$ the appropriate split is

$$\mathbf{E}_{\rm I} + \mathbf{E}_{\rm II} = \begin{bmatrix} 0 & E_{12} & E_{13} \\ E_{12} & 0 & E_{23} \\ E_{13} & E_{23} & E_{33} \end{bmatrix} + \begin{bmatrix} E_{11} & 0 & 0 \\ 0 & E_{22} & 0 \\ 0 & 0 & 0 \end{bmatrix}. \tag{52}$$

For isotropic material this becomes

$$\mathbf{E}_{\rm I} + \mathbf{E}_{\rm II} = E \begin{bmatrix} 0 & \nu & 0 \\ \nu & 0 & 0 \\ 0 & 0 & \frac{1}{2}(1-\nu) \end{bmatrix} + E \begin{bmatrix} 1 & 0 & 0 \\ 0 & 1 & 0 \\ 0 & 0 & 0 \end{bmatrix}, \tag{53}$$

which agrees with (51) for zero Poisson's ratio, as may be expected. Some FEM books suggest using the deviatoric and dilatational elasticity laws for $\mathbf{E}_I$ and $\mathbf{E}_{II}$, respectively. As can be seen, that recommendation is incorrect for this element.

§5.8. Slender Isotropic Cantilever

No matter how good it looks on paper, any new quadrilateral element should be first tested on the slender cantilever benchmark depicted in Figure 13. This is primarily intended to confirm the results of the energy ratio test. The 16:1 cantilever beam of Figure 13(a) is fabricated of isotropic material, with $E = 7680$, $\nu = 1/4$ and $G = (2/5)E = 3072$. The dimensions are shown in the figure. Two end load cases are considered: an end moment $M = 1000$ and a transverse end shear $P = 48000/1027 = 46.7381$. Both tip deflections $\delta_C = u_{yC}$ from beam theory: $ML^2/(2EI_z)$ and $PL^3/(3EI_z) + PL/(GA_s)$, in which $I_z = b^3h/12$ and $A_s = 5A/6 = 5bh/6$, are exactly 100. For the second load case the shear deflection is only 0.293% of u_{yC}; thus the particular expression used for A_s is not important.

Regular meshes with only one element ($N_y = 1$) through the beam height are considered. The number N_x of elements along the span is varied from 1 to 64, giving elements with aspect ratios from $\gamma = 16$ through $\gamma = \frac{1}{4}$. The root clamping condition is imposed by setting u_x to zero at both root nodes, but u_y is only fixed at the lower one thus allowing for Poisson's contraction at the root.

Tables 3 and 4 report computed tip deflections u_{yC} for several element types. The first three rows list results for the 3 rectangular panel models of Table 2. The last three rows give results for selected

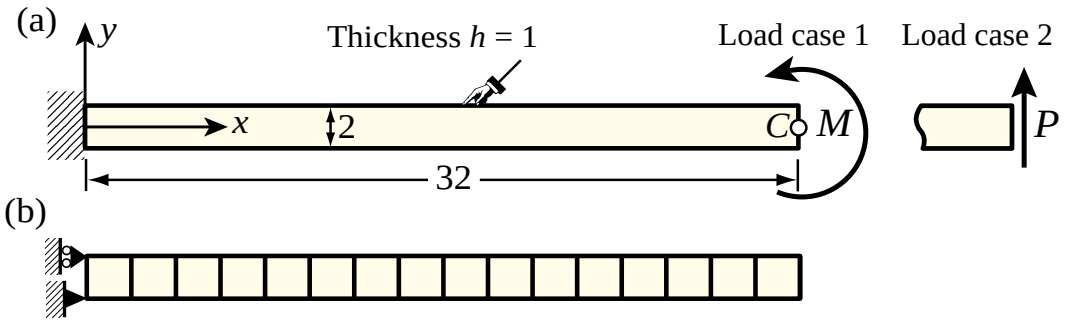

FIGURE 13. Slender cantilever beam for benchmark tests discussed in §5.8 and §5.9. A 16×1 FEM mesh with $\gamma = 1$ is shown in (b).

triangular elements. BODT is the Bending Optimal Drilling Triangle: a 3-node membrane element with drilling freedoms studied in previous papers [2,16,17,26]. ALL-EX is the exactly integrated 1988 Allman triangle with drilling freedoms [1]. CST is the Constant Strain Triangle, also called linear triangle and Turner triangle [61]. Both ALL-EX and BODT have three freedoms per node whereas all others have two. To get exactly 100.00% from BODT under a end-moment loading requires paying particular attention to force lumping [17].

StressRP is exact for any γ under end-moment and converges rapidly under end-shear. The performance of BODT is similar, inasmuch it is constructed to be bending exact in rectangular-mesh units. (In the end-shear load case StressRP and BODT, which morph to different beam templates, converge to slightly different limits as $\gamma \to 0$.) StrainRP is about 6% stiffer than StressRP, which can be expected since $1/(1-\nu^2) = 16/15$. DispRP, as well as triangles ALL-EX and CST, locks as γ increases.

The response for more element layers through the height can be readily estimated from equation (45). Thus those results are omitted. For example, to predict the DispRP answer on a 8×4 mesh under end-moment, proceed as follows. The aspect ratio is $\gamma = 8$. From the $\gamma = 8$ column of Table 3 read off $r_x = 100/3.75 = 26.667$. Set $n = 2$ in (45) to get $r_x^{(4)} = (15 + r_x)/16 = 2.60417$. The estimated tip deflection is $100/2.60417 = 38.40$. Running the program gives $\delta_C = 38.3913$ as average of the y displacement of the two end nodes. Predictions for the end-shear-load case will be less accurate but sufficient for quick estimation.

§5.9. Slender Anisotropic Cantilever

Benchmarks with anisotropic material properties are rarely reported in the FEM literature. A particularly insidious one results by taking the beam of Figure 13(a) as fabricated of anisotropic material with the elasticity properties

$$\mathbf{E} = \begin{bmatrix} 880 & 600 & 250 \\ 600 & 420 & 150 \\ 250 & 150 & 480 \end{bmatrix}, \quad \mathbf{C} = \mathbf{E}^{-1} = \frac{1}{35580}\begin{bmatrix} 1791 & -2505 & -150 \\ -2505 & 3599 & 180 \\ -150 & 180 & 96 \end{bmatrix}. \tag{54}$$

That these are physically realizable can be checked by getting the eigenvalues of $\mathbf{E}$: {1386.1, 387.3, 6.63}, whence both $\mathbf{E}$ and $\mathbf{C}$ are positive definite. The load magnitudes are adjusted to get beam-theory tip deflections of 100: $M = 2.58672$ and $P = 0.121153$. Since $E_{11}C_{11} = 44.297$ the energy ratio analysis of §5.4 and §5.5, through (42) and (43), predicts that the strain and displacement models will be big losers, because $r_x \geq 44.297$. This is verified in Tables 5 and 6, which report computed tip deflections u_{yC} for the three models of Table 2. While StressRP shines, the strain and displacement models are way off, regardless of how many elements are placed along x.

Table 3 Tip Deflections (exact=100) for Slender Isotropic Cantilever under End Moment

Element	Mesh: x-subdivisions $\times$ y-subdivisions ($N_x \times N_y$)						
	1×1 ($\gamma = 16$)	2×1 ($\gamma = 8$)	4×1 ($\gamma = 4$)	8×1 ($\gamma = 2$)	16×1 ($\gamma = 1$)	32×1 ($\gamma = \frac{1}{2}$)	64×1 ($\gamma = \frac{1}{4}$)
StressRP	100.00	100.00	100.00	100.00	100.00	100.00	100.00
StrainRP	93.75	93.75	93.75	93.75	93.75	93.75	93.75
DispRP	0.97	3.75	13.39	37.49	68.18	85.71	91.60
ALL-EX	0.04	0.63	7.40	35.83	58.44	64.89	66.45
CST	0.32	1.25	4.46	12.50	22.73	28.57	30.53
BODT	100.00	100.00	100.00	100.00	100.00	100.00	100.00

Table 4 Tip Deflections (exact=100) for Slender Isotropic Cantilever under End Shear

Element	Mesh: x-subdivisions $\times$ y-subdivisions ($N_x \times N_y$)						
	1×1 ($\gamma = 16$)	2×1 ($\gamma = 8$)	4×1 ($\gamma = 4$)	8×1 ($\gamma = 2$)	16×1 ($\gamma = 1$)	32×1 ($\gamma = \frac{1}{2}$)	64×1 ($\gamma = \frac{1}{4}$)
StressRP	75.02	93.72	98.39	99.56	99.86	99.94	99.97
StrainRP	70.35	87.88	92.26	93.35	93.63	93.71	93.73
DispRP	0.97	3.75	13.39	37.49	68.16	85.69	91.58
ALL-EX	0.24	0.69	6.36	35.18	59.59	65.70	67.03
CST	0.48	1.41	4.62	12.66	22.88	28.73	30.69
BODT	75.20	93.37	98.20	99.55	99.93	100.12	100.15

Table 5 Tip Deflections (exact=100) for Slender Anisotropic Cantilever under End Moment

Element	Mesh: x-subdivisions $\times$ y-subdivisions ($N_x \times N_y$)						
	1×1 ($\gamma = 16$)	2×1 ($\gamma = 8$)	4×1 ($\gamma = 4$)	8×1 ($\gamma = 2$)	16×1 ($\gamma = 1$)	32×1 ($\gamma = \frac{1}{2}$)	64×1 ($\gamma = \frac{1}{4}$)
StressRP	100.00	100.00	100.00	100.00	100.00	100.00	100.00
StrainRP	2.26	2.26	2.26	2.26	2.26	2.26	2.26
DispRP	0.02	0.07	0.25	0.76	1.53	2.08	2.25

Table 6 Tip Deflections (exact=100) for Slender Anisotropic Cantilever under End Shear

Element	Mesh: x-subdivisions $\times$ y-subdivisions ($N_x \times N_y$)						
	1×1 ($\gamma = 16$)	2×1 ($\gamma = 8$)	4×1 ($\gamma = 4$)	8×1 ($\gamma = 2$)	16×1 ($\gamma = 1$)	32×1 ($\gamma = \frac{1}{2}$)	64×1 ($\gamma = \frac{1}{4}$)
StressRP	74.95	93.68	98.37	99.54	99.84	99.92	99.96
StrainRP	1.70	2.12	2.22	2.26	2.26	2.26	2.26
DispRP	0.02	0.07	0.25	0.75	1.52	2.06	2.23

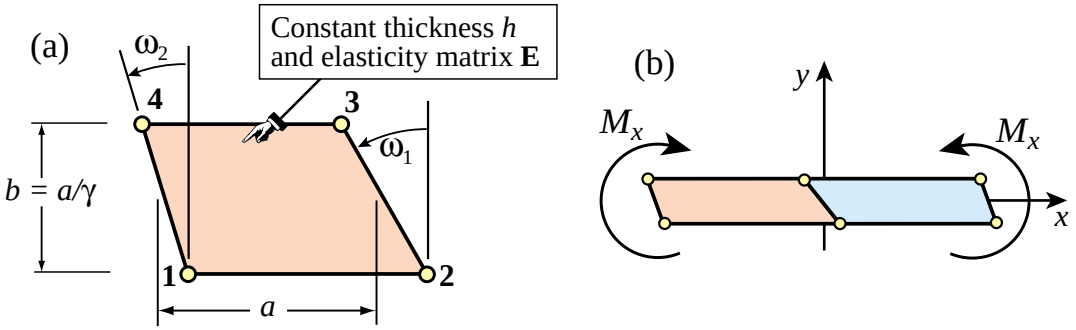

FIGURE 14. Trapezoidal panel shape: (a) individual trapezoid geometry; (b) a two-trapezoid repeatable macroelement.

Putting more layers through the height will help StrainRP and DispRP but too slowly to be practical. For example, a 128×8 mesh of StrainRP (or clones) under end moment will have $r_x^{(8)} = (63{+}44.297)/64 = 1.676$ and estimated $u_{yC} = 100/1.676 = 59.647$. Running that mesh gives $u_{yC} = 59.65$. So using over 2000 freedoms in this fairly trivial problem the results are still off by about 40%.

§6. Specialization 2: The Trapezoidal Panel

The rectangular panel template has instructional value, but none as new technology driver. The optimal element of this geometry, StressRP, was published in 1956 [61] and it has been cloned many times since, as Table 2 makes clear.

Template power as generator of new customized elements emerges when one passes to more general geometries. The trapezoidal panel (TP) pictured in Figure 14(a) is a case in point. A trapezoid has two parallel opposite sides but the angles ω_1 and ω_2 are arbitrary. What is the bending-optimal element of this shape? This question can be answered by studying the repeating macroelement shown in Figure 14(b). It is obtained by gluing two mirror-image trapezoids to form a parallelogram. By "repeating" is meant that this macroelement can tile the entire $\{x, y\}$ plane by repetition.

If $a >> b$ and $\omega_1 \neq \omega_2$ the assumed stress fabricated macroelement (StressTP) rapidly becomes overstiff and overflexible in x- and y-bending, respectively. For example if $a/b = \gamma = 8$, $\omega_1 = 0$, $\tan\omega_2 = 1/2$ and isotropic material with $\nu = 1/4$ the bending ratios are $r_x = 11.97$ and $r_y = 0.1414$. For the anisotropic elasticity matrix (54), $r_x = 6.93$ and $r_y = 0.0792$. If an elongated macroelement is supposed to model unidirectional x-bending correctly, the overstiffness caused by $\omega_1 \neq \omega_2$ is called *distortion locking*. This phenomenon has been widely studied since the MacNeal-Harder test suite gained popularity [39].

Using the template (34)–(35) it is possible to construct an element that is exact in unidirectional x bending when configured to form a repeatable macroelement as in Figure 14(b), for any aspect ratio $\gamma = a/b$ as well as arbitrary angles ω_1 and ω_2. This instance will be called UBOTP (for Unidirectional Bending Optimal Trapezoidal Panel). If $\omega_1 = \omega_2 = 0$ this reduces to the optimal rectangular panel StressRP discussed in Section 5.1, as can be expected. However this particular element cannot be constructed by any formulation currently known to the writer. It simply results from appropriately setting the entries of $\mathbf{W}$ and $\mathbf{R}$ so that exact bending response is reproduced. The expression of $\mathbf{R}$ is considerably simplified by writing it in terms of entries of the natural compliance matrix $\breve{\mathbf{C}}$ introduced in Section 3.4. Detailed expressions are given in the Appendix of [27].

It is not difficult to prove, using a computer algebra system, that $\mathbf{W}^T\mathbf{R}\mathbf{W}$ for UBOTP is positive definite

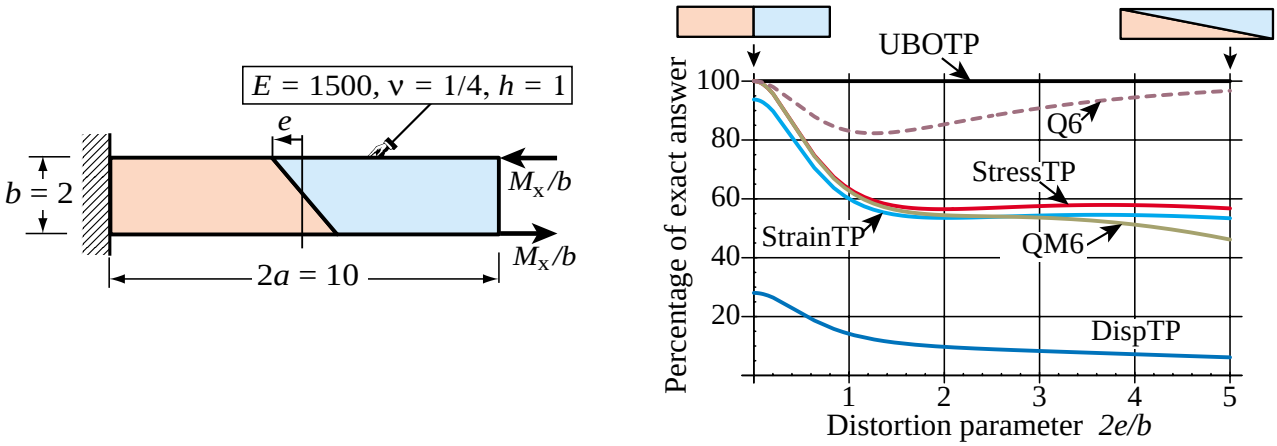

FIGURE 15. A well known plane stress distortion benchmark. Dashed lines mark elements that fail the patch test (only Q6 in this particular test set).

as long as the trapezoid is convex. Not only that: its condition number is bounded, which is another way of saying that the inf-sup — also called LBB condition — is verified. Consequently the element stiffness is nonnegative, and has the correct rank.

Figure 15 presents results for a widely used mesh distortion test, which involves applying an end moment to one macroelement of the type discussed. Results for six element instances: UBOTP, StressTP, StrainTP, DispTP, Q6 and QM6 are shown. The percentage of the correct answer is of course $100/r_x$. Each model but Q6 was implemented as instance of the template (34)–(35), whereas Q6 (which is not a template instance because it fails the patch test) was coded separately. All computations were done symbolically by the same *Mathematica* module and the deflection was returned as an analytical function of e/b. This explains why the curves in Figure 15 are smooth.

Of these six models only Q6 fails the patch test, but otherwise works better than all others but UBOTP. StressTP, StrainTP and QM6 give similar results, as can be expected, whereas DispTP is way overstiff even for zero distortion. UBOTP gives the correct result for all distortion parameters from 0 through 5, since $r_x \equiv 1$. If the aspect ratio of the cantilever is changed to, say $2a/b = 10$, the differences between elements become more dramatic.

For distortion performance results on other models such as Pian-Sumihara and Enhanced Assumed Strain, see Lautersztajn and Samuelsson [37]. There exists a penalty-augmented modification of the Pian-Sumihara quadrilateral constructed by Wu and Cheung [63] that achieves distortion insensitivity at the cost of rank deficiency.

At first sight the existence of UBOTP contradicts a theorem by MacNeal [41], which says that four noded quadrilaterals cannot simultaneously pass the patch test and be insensitive to distortion. The escape hatch is that y-bending optimality (along the skew angular direction ω_1 of the macroelement) is not attempted. If one tries imposing $r_x = r_y = 1$, the solutions for $\{R_{11}, R_{12}, R_{22}\}$ become complex if $\gamma >> 1$ as soon as the angular difference $\omega_2 - \omega_1$ deviates slightly from zero.

§7. Historical Overview

The 4-node, 8-DOF membrane (plane stress) flat quadrilateral is one of the most interesting finite elements from the standpoint of its persistent influence on theory and practice of "finitelementology." In what follows "panel" as usual is an abbreviation for "thin plate in plane stress."

§7.1. The Rectangular Panel

As an assumed displacement model the 4-noded rectangular panel was first published by J. H. Argyris in his celebrated 1954 serial [3]. It appears on page 62 of the Butterworths reprint. The model incorporated edge reinforcements, since it was intended to model stiffened cover plates in aircraft wings and fuselages. The derivation of the stiffness matrix used Castigliano's first theorem to produce the stiffness influence coefficients. This is a classical tool in structural mechanics. The novel ingredient was the kinematic assumption: a bilinear interpolation of in-plane displacements in Cartesian coordinates aligned with the rectangle edges. The first continuum-based, displacement-assumed element was born.

At that time the issue of interelement continuity had not arisen. It became important much later, especially as the idea was extended to plate bending. In Argyris' model, inter-rectangle conformity was automatically met because the bilinear displacement variation reduces to a linear one over each side.

A 4-node flat rectangular panel was constructed in 1952–53 by Turner's research group at Boeing [12] but was not published until 1956 [61]. The derivation method was completely different. It begins with interelement stress-flux assumptions combining five "load states" that if extended into the element would produce 3 constant stress and 2 bending stress modes. From these a flexibility matrix is obtained and inverted to furnish a deformational stiffness. This is expanded with rigid body modes to yield the free-free stiffness matrix. In current terminology, it was a stress-assumed element, and coincides with the so-called StressRP template of Section 5. As shown there this *is* the optimal rectangular panel, which is a tribute to the physical insight of that small but high-caliber research team.

Thus two dual formulation approaches: assumed stress versus displacement, or equilibrium versus kinematics, can be seen in action since the mid-1950s for this particular element configuration. Questions of consistency, convergence and bounding were not yet well understood. The missing ingredient was connection to direct variational methods and in particular Rayleigh-Ritz. The link was clearly established in Melosh's thesis of 1962 [42] and his subsequent paper [43].

§7.2. The Quadrilateral Panel

Extension to parallelograms is not difficult using skew Cartesian coordinates. A closed form solution, discussed in detail by Gallagher in his 1963 review [28], is possible. The extension to quadrilateral shapes was, however, slow in coming. In the meantime the modeling need had been alleviated by using macroelements fabricated with four Turner triangles, an approach also presented in [61]. This has the benefit of automatically taking care of warped panels, in which the four corners do not lie on a plane.

A direct construction with assumed displacements was pursued by I. C. Taig at English Electric Aviation (later British Aerospace) since 1957 [35, p. 520]. The element was finally presented at an AGARD 1962 meeting, and appeared in print two years later [59]. The key enabling tool was the use of bilinear interpolation in body-fitted dimensionless coordinates. These were labeled ξ and η, as quadrilateral natural coordinates now are, but ran from 0 to 1. The stiffness matrix was derived in closed form, which was an amazing *tour de force* in days before computer algebra systems. (This grueling effort may have partly accounted for the long publication delay.)

In the same AGARDOgraph volume Argyris, Kelsey and Kamel [4] used a Cartesian expansion to attack the general quadrilateral shape. They recognize the lack of interelement continuity — the effects of which were only beginning to be understood — and remark that a solution such as Taig's could be used to remedy that problem.

Bruce Irons, who was aware of Taig's work while at the Rolls Royce aircraft division (the FEM world, then nucleated in Aerospace, was tiny; everybody was aware of what others were doing) developed the far-reaching isoparametric extension for arbitrary elements upon moving to Swansea [34,35].

§7.3. Hybrids

The novel hybrid stress formulation of Pian appeared in the mid 1960s [49,50]. A theoretical basis in the form of variational principles was presented in 1970 by Pian and Tong [51]. For this particular element the formulation was initially restricted to the rectangular shape, since lack of invariance (due to use of stress assumptions in Cartesian coordinates) made extensions difficult. The end result for the rectangular panel was identical to that obtained by Turner et. al. in 1956 [61]. Curiously the coalescence was not fully explained until 36 years later [53]. The first correct and invariant hybrid formulation for general quadrilateral geometry using natural stresses, by Pian and Sumihara, appeared in 1984 [52]. This was an influential discovery that finally placed the stress-assumed approach on a par with isoparametrics.

§7.4. Unlocking Remedies

The poor performance of the Taig quadrilateral for in-plane bending due to "shear locking" motivated investigators to introduce a number of cures: selective and reduced integration, incompatible modes, assumed strains, the $\bar{\mathbf{B}}$ formulation for near-incompressible materials, etc. Most of them are well covered in Hughes' textbook [33]. Several of those remedies were subsequently extended to more general structural models such as plate bending, shells and three dimensional solids. Thus the quadrilateral panel did serve both as motivator and testbed of new finite element technologies.

In addition to shear locking, both original and improved 4-node quadrilateral models were observed to be prone to *distortion locking*. This is bending overstiffness caused by deviation from a rectangular or parallelogram shape. An important result of MacNeal, hinted at in [40] and published as a theorem in 1987 [41], sets out a serious limitation: a four noded plane stress element cannot both pass the patch test for any configuration and be insensitive to distortion when subject to in-plane bending. Indeed all elements published to date do comply with the theorem, as surveyed in [37]. The UBOTP element discussed in Section 6, which passes the patch test, circumvents it only partially, in that in-plane bending optimality is obtained only along one direction. (This is not much of a limitation, because in high-aspect-ratio quadrilaterals flexural overstiffness tends to be more pronounced along the *long element direction*, which can be found by comparing the two median lengths.)

§7.5. Tradeoffs

A interesting open question in recent element-level research concerns the tradeoff between two desirable requirements: passing the patch test for arbitrary geometries versus low distortion sensitivity. Physically the patch test enforces mean flux conservation conditions across interelement boundaries. Such conditions work as constraints that may impede desirable element motions in distorted elements.

As noted above, for the 4-noded quadrilateral panel an in-depth study was recently reported in [37]. The focus of that survey was on the classical distortion benchmark of Figure 15. As can be expected from MacNeal's theorem, elements that did not pass the patch test, such as Q6, did relatively well compared

to those that pass it for any geometry. An argument advanced by several authors in favor of alleviating distortion sensitivity is that the patch test need only be passed in the limit of a mesh subdivision process that eventually converges to elements of parallelogram or rectangular shape. Consequently enforcing the patch test for *any* geometry seems overly restrictive. Arguments on either side of the issue can be expected to come forward in the near future.

The writer's opinion is that requiring satisfaction of the patch test for arbitrary shapes should take first priority, because often this is the only way to check individual elements as well as (even more importantly) interfacing different element types such as shells, solids and beams. Furthermore in many engineering projects involving complex structures meshes are never refined, so the argument of indefinite subdivision becomes tenuous. The design of templates, which enforce the IET of [7] *a priori*, responds to this assessment of priorities.

§8. Conclusions

This is the second stiffness template developed by the writer using the "supernatural" approach, in which *all* element field equations: kinematic, equilibrium and constitutive, are expressed in both Cartesian and natural coordinates. The first template pertains to a 3-node triangle with drilling corner freedoms, recently reformulated in [26]. Although it can be argued that two case studies dont make a representative sample, it seems appropriate to summarize here what has been learned so far. Certainly going natural all the way involves additional preparatory work. This can be arduous and exacting, as the Appendix material makes clear. (In fact that work would have been impossible without the help of a computer algebra system.) The obvious question comes up: is this extra effort worthwhile?

The answer has to be qualified. Recall that a template such as (34) is the sum of two components: basic and higher order stiffness. There is no doubt in the writer's mind that the natural approach simplifies the construction of the latter, and that the extra preparation pays off handsomely in the end. Obtaining a form such as that of Figure 10, which displays the separation of formulation dependent and independent parts, would be exceedingly difficult — not to say impossible — in a Cartesian framework.

For the basic stiffness component, however, another factor comes into play. Does the element possess a constant natural metric, as is the case for 3-node triangles and 4-node parallelograms, or can it have variable metric, as in arbitrarily shaped quadrilaterals? The two cases must be distinguished because the basic stiffness characterizes the response to *uniform* states.

(1) Constant element metric means that a uniform Cartesian strain state maps to *constant* natural strains. The basic stiffness should be exactly the same with either approach. The Cartesian framework, however, does not entail extra preparation work and ought to be favored for expediency.

(2) Variable element metric means that a uniform Cartesian strain maps to a *variable* natural strain field. The mapped field can be exceedingly complicated, for example rational functions of the natural coordinates. But if the developer mistakingly replaces it by a constant natural strain state, the patch test may be violated. So the safest choice is to stay Cartesian.

The recommended strategy is clear-cut: *stay Cartesian for the basic stiffness, but go natural for the higher order one*. Historical tradition, however, clouds this advice. Most element formulations are designed to produce the total stiffness in one shot, without decomposition. Developers who follow this well traveled path are soon caught in a dilemma:

(C) Stay Cartesian all the way. This risks getting mired with poorly performing or non-invariant elements. (The latter defect actually held up advances of stress hybrids for 20 years).

(N) Go natural all the way and risk violation of the patch test.

In practice a compromise may be struck: go natural part way but revert to Cartesian at a certain point of the derivation. The isoparametric formulation of Irons and coworkers provides an early example. Shape functions and element geometry are expressed in terms of natural coordinates; but everything else: displacements, strains, stresses, energy, load distributions, etc, is kept Cartesian. Researchers in the 1980s timidly stepped further. For example, Pian-Sumihara's "natural hydrid" formulation uses natural stresses but leaves constitutive equations Cartesian.

At which point does one draw the line? For the total stiffness, one-shot formulation there is no clear answer. It is rolling the dice. A developer tries something, builds an element, implements it and does *a posteriori* checks. If the element violates invariance, go natural further. If it violates the patch test, turn back to Cartesian earlier. And so on. With luck a working element may emerge, but there is no assurance that it is not a clone of something previously published.

To summarize, *lack of understanding about kinematic divide-and-conquer has hurt the progress of natural methods*. By itself the tool is not at fault. It has to be used on the right context and limited to where it works best.

These comments have to be tempered in situations where a kinematic decomposition is not obvious. The classical example is that of doubly curved shell elements, in which the separation of constant states of strains and curvatures remains a matter of debate, as also is the precise meaning of shell patch tests. For simpler scenarios, however, the decomposition procedure is clearly defined.

Can the natural approach be extended to nonlinear problems? That question was posed by a reviewer familiar with Argyris' struggles in extending his "Urelements" [5] into the large strain range. As expected no difficulties arise if deformations stay small. Small-strain elements, whether developed by templates or not, can be smoothly fitted into a corotational approach to take care of large rotations. This was first done by Nygård [46] for Free Formulation shell elements. Introduction of small-strain material nonlinearities is also straightforward. Collectively these scenarios cover many practical applications.

To the writer's knowledge, however, nobody has tried to generalize the motion decomposition of Figure 7 to derive finite-strain elements. It can be done in principle in the form of multiplicative splits facilitated by the polar decomposition theorem. For example, a finite rigid-body motion followed by uniform stretching and finalized with deviatoric deformations. But serious obstacles appear on the path: formidable mathematics required to derive natural relations, and the loss of safety blankets such as the patch test and energy orthogonality. Whether the natural approach can contribute to finite element technology for this class of problems is an open question.

Appendix A. QUADRILATERAL PROPERTIES

A.1 Geometry

The geometry of a flat, straight-sided quadrilateral is defined by the four corner coordinates $\{x_i, y_i\}$, $i = 1, 2, 3, 4$. See Figure 16(a). We shall employ the abbreviations $x_{ij} = x_i - x_j$ and $y_{ij} = y_i - y_j$ for node coordinate differences.

The coordinates of the corner average are $x_0 = \frac{1}{4}(x_1 + x_2 + x_3 + x_4)$ and $y_0 = \frac{1}{4}(y_1 + y_2 + y_3 + y_4)$. These define the position of the quadrilateral center 0. Side midpoints are identified by labels 5, 6, 7 and 8, assigned as shown in Figure 16(b). The signed quadrilateral area is denoted by $A = \int_{\Omega^e} d\Omega$. This is identified below with the coefficient A_0 (which comes from the Jacobian determinant expression) for notational convenience.

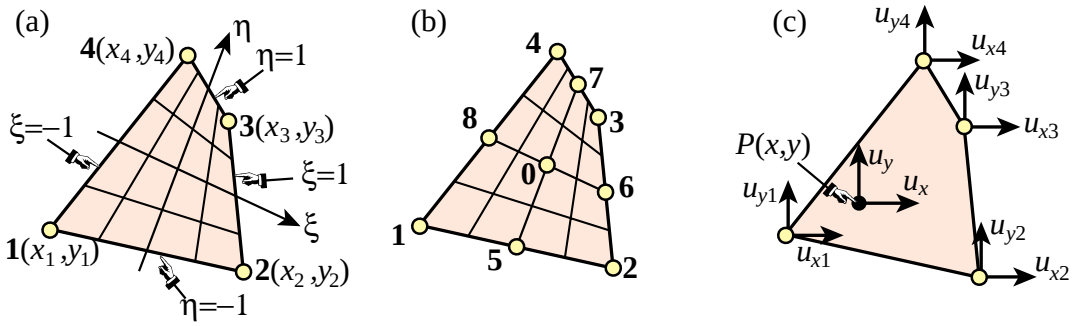

FIGURE 16. Quadrilateral geometric and kinematic properties: (a) natural coordinates; (b) midpoint and center point numbering, (c) Cartesian displacements of a generic point P and node displacements.

The well known natural coordinates are ξ and η, which range from -1 to $+1$. These are pictured in Figure 16(a). The quadrilateral geometry is defined isoparametrically:

$$x(\xi,\eta) = \sum\nolimits_{i=1}^{4} x_i\, N_i(\xi,\eta), \qquad y(\xi,\eta) = \sum\nolimits_{i=1}^{4} y_i\, N_i(\xi,\eta) \tag{55}$$

in which $N_i = \frac{1}{4}(1 \pm \xi)(1 \pm \eta)$ are the bilinear shape functions.

Three invariants with dimension of area that often appear in subsequent formulas are

$$A_0 = A = \tfrac{1}{2}(x_{31}y_{42} - x_{42}y_{31}), \quad A_1 = \tfrac{1}{2}(x_{34}y_{12} - x_{12}y_{34}), \quad A_2 = \tfrac{1}{2}(x_{23}y_{14} - x_{14}y_{23}). \tag{56}$$

Denote by A_{ijk} the signed area of the triangle spanned by the 3 corners $\{i, j, k\}$. These are linked to the A_i as follows:

$$\begin{aligned}
A_{123} &= \tfrac{1}{2}(A_0 + A_1 - A_2) = \tfrac{1}{2}(x_{21}y_{32} - x_{32}y_{21}) = \tfrac{1}{2}(x_{13}y_{21} - x_{21}y_{13}),\\
A_{234} &= \tfrac{1}{2}(A_0 + A_1 + A_2) = \tfrac{1}{2}(x_{32}y_{43} - x_{43}y_{32}) = \tfrac{1}{2}(x_{24}y_{32} - x_{32}y_{24}),\\
A_{341} &= \tfrac{1}{2}(A_0 - A_1 + A_2) = \tfrac{1}{2}(x_{43}y_{14} - x_{14}y_{43}) = \tfrac{1}{2}(x_{31}y_{43} - x_{43}y_{31}),\\
A_{412} &= \tfrac{1}{2}(A_0 - A_1 - A_2) = \tfrac{1}{2}(x_{14}y_{21} - x_{21}y_{14}) = \tfrac{1}{2}(x_{42}y_{14} - x_{14}y_{42}),\\
A_0 &= A = A_{123} + A_{341} = A_{234} + A_{412},\\
A_1 &= A_{234} - A_{341} = A_{123} - A_{412},\\
A_2 &= A_{341} - A_{412} = A_{234} - A_{123}.
\end{aligned} \tag{57}$$

In the following subsection it will be seen that the Jacobian determinant can be expressed as $J = (A_0 + A_1\xi + A_1\eta)/4$. Its value at corner 1 is $(A_0 - A_1 - A_2)/4 = A_{412}/2$. Similarly at corners 2, 3 and 4 the values of J are $A_{123}/2$, $A_{234}/2$ and $A_{341}/2$, respectively. The following identities are easily verified algebraically:

$$\begin{bmatrix} x_{14} & x_{42} & x_{34} & 0\\ x_{13} & x_{32} & 0 & x_{34}\\ x_{12} & 0 & x_{32} & x_{24}\\ 0 & x_{12} & x_{31} & x_{14}\end{bmatrix}\begin{bmatrix} A_{234}\\ A_{341}\\ A_{412}\\ A_{123}\end{bmatrix} = \begin{bmatrix}0\\0\\0\\0\end{bmatrix}, \quad \begin{bmatrix} y_{14} & y_{42} & y_{34} & 0\\ y_{13} & y_{32} & 0 & y_{34}\\ y_{12} & 0 & y_{32} & y_{24}\\ 0 & y_{12} & y_{31} & y_{14}\end{bmatrix}\begin{bmatrix} A_{234}\\ A_{341}\\ A_{412}\\ A_{123}\end{bmatrix} = \begin{bmatrix}0\\0\\0\\0\end{bmatrix},$$
$$\begin{bmatrix} 1 & 1 & 1 & 1\\ x_1 & x_2 & x_3 & x_4\\ y_1 & y_2 & y_3 & y_4\end{bmatrix}\begin{bmatrix} -A_{234}\\ A_{341}\\ -A_{412}\\ A_{123}\end{bmatrix} = \begin{bmatrix}0\\0\\0\end{bmatrix}, \quad \begin{bmatrix} x_{12}+x_{34} & x_{13}+x_{24} & x_{12}+x_{43}\\ y_{12}+y_{34} & y_{13}+y_{24} & y_{12}+y_{43}\\ x_{14}+x_{32} & x_{14}+x_{23} & x_{13}+x_{42}\\ y_{14}+y_{32} & y_{14}+y_{23} & y_{13}+y_{42}\end{bmatrix}\begin{bmatrix} A_0\\ A_1\\ A_2\end{bmatrix} = \begin{bmatrix}0\\0\\0\\0\end{bmatrix}. \tag{58}$$

$$\begin{bmatrix} -x_{14} & x_{21} \\ -y_{14} & y_{21} \\ x_{32} & x_{21} \\ y_{32} & y_{21} \\ x_{32} & -x_{43} \\ y_{32} & -y_{43} \\ -x_{14} & -x_{43} \\ -y_{14} & -y_{43} \end{bmatrix} \begin{bmatrix} A_1 \\ A_2 \end{bmatrix} = 2 \begin{bmatrix} A_{412}x_{12|34} \\ A_{412}y_{12|34} \\ A_{123}x_{12|34} \\ A_{123}y_{12|34} \\ A_{234}x_{12|34} \\ A_{234}y_{12|34} \\ A_{341}x_{12|34} \\ A_{341}y_{12|34} \end{bmatrix}, \quad \begin{bmatrix} x_{21} & -x_{24} & 0 \\ y_{21} & -y_{24} & 0 \\ x_{21} & x_{31} & 0 \\ y_{21} & y_{31} & 0 \\ -x_{43} & -x_{42} & 0 \\ -y_{43} & -y_{42} & 0 \\ -x_{43} & x_{13} & 0 \\ -y_{43} & y_{13} & 0 \\ -x_{14} & 0 & x_{24} \\ -y_{14} & 0 & y_{24} \\ x_{32} & 0 & -x_{31} \\ y_{32} & 0 & -y_{31} \\ x_{32} & 0 & x_{42} \\ y_{32} & 0 & y_{42} \\ -x_{14} & 0 & -x_{13} \\ -y_{14} & 0 & -y_{13} \end{bmatrix} \begin{bmatrix} A_0 \\ A_1 \\ A_2 \end{bmatrix} = 2 \begin{bmatrix} A_{412}x_{21|34} \\ A_{412}y_{21|34} \\ A_{123}x_{21|34} \\ A_{123}y_{21|34} \\ A_{234}x_{21|34} \\ A_{234}y_{21|34} \\ A_{341}x_{21|34} \\ A_{341}y_{21|34} \\ A_{412}x_{32|41} \\ A_{412}y_{32|41} \\ A_{123}x_{32|41} \\ A_{123}y_{32|41} \\ A_{234}x_{32|41} \\ A_{234}y_{32|41} \\ A_{341}x_{32|41} \\ A_{341}y_{32|41} \end{bmatrix} \tag{59}$$

In (59), $x_{12|34} = (x_{12}+x_{34})/2$, $y_{12|34} = (y_{12}+y_{34})/2$, $x_{21|34} = (x_{21}+x_{34})/2$, $y_{21|34} = (y_{21}+y_{34})/2$, $x_{32|41} = (x_{32}+x_{41})/2$ and $y_{32|41} = (y_{32}+y_{41})/2$. Four of these can be interpreted as $\{x, y\}$ components of the quadrilateral median segments 6-8 and 7-5: $x_{21|34} = x_{68}$, $y_{21|34} = y_{68}$, $x_{32|41} = x_{75}$ and $y_{32|41} = y_{75}$.

A.2 Metric Relations

The metric transformations between Cartesian and natural coordinates are

$$\begin{bmatrix} dx \\ dy \end{bmatrix} = \begin{bmatrix} \partial x/\partial\xi & \partial x/\partial\eta \\ \partial y/\partial\xi & \partial y/\partial\eta \end{bmatrix} \begin{bmatrix} d\xi \\ d\eta \end{bmatrix} = \mathbf{J}^T \begin{bmatrix} d\xi \\ d\eta \end{bmatrix}, \quad \begin{bmatrix} d\xi \\ d\eta \end{bmatrix} = \begin{bmatrix} \partial\xi/\partial x & \partial\xi/\partial y \\ \partial\eta/px & \partial\eta/\partial y \end{bmatrix} \begin{bmatrix} dx \\ dy \end{bmatrix} = \mathbf{J}^{-T} \begin{bmatrix} dx \\ dy \end{bmatrix}. \tag{60}$$

Here $\mathbf{J}$ denotes the Jacobian matrix of $\{x, y\}$ with respect to $\{\xi, \eta\}$:

$$\mathbf{J} = \frac{\partial(x, y)}{\partial(\xi, \eta)} = \begin{bmatrix} \partial x/\partial\xi & \partial y/\partial\xi \\ \partial x/\partial\eta & \partial y/\partial\eta \end{bmatrix} = \begin{bmatrix} J_{11} & J_{12} \\ J_{21} & J_{22} \end{bmatrix}. \tag{61}$$

This definition of $\mathbf{J}$ is that used by most authors; nevertheless some take $\mathbf{J}$ as the transpose of the above. Replacing the shape functions yields

$$\begin{aligned} 4J_{11} &= 4\partial x/\partial\xi = x_{21} + x_{34} + (x_{12} + x_{34})\eta, \quad 4J_{12} = 4\partial y/\partial\xi = y_{21} + y_{34} + (y_{12} + y_{34})\eta, \\ 4J_{21} &= 4\partial x/\partial\eta = x_{32} + x_{41} + (x_{12} + x_{34})\xi, \quad 4J_{22} = 4\partial y/\partial\eta = y_{32} + y_{41} + (y_{12} + y_{34})\xi. \end{aligned} \tag{62}$$

The Jacobian determinant can be expressed in invariant form as

$$\begin{aligned} J = \det(\mathbf{J}) = J_{11}\,J_{22} - J_{12}J_{21} &= \tfrac{1}{4}(A_0 + A_1\xi + A_2\eta), \quad \text{with} \quad A_0 = A, \\ A_1 = \tfrac{1}{2}(x_{34}y_{12} - x_{12}y_{34}) = A_{234} - A_{341}, &\quad A_2 = \tfrac{1}{2}(x_{23}y_{14} - x_{14}y_{23}) = A_{341} - A_{412}. \end{aligned} \tag{63}$$

If $A_1 = A_2 = 0$ the element is said to have *constant metric* because if so $J = A_0/4$ does not depend on $\{\xi, \eta\}$. The quadrilateral then reduces to a rectangle or parallelogram.

Let $\{x_C, y_C\}$, $\{\xi_C, \eta_C\}$, $\{x_D, y_D\}$ and $\{\xi_D, \eta_D\}$ denote Cartesian and natural coordinates of the quadrilateral areal centroid C and of the intersection of the diagonals D. It can be verified that

$$\begin{aligned} &x_C - x_0 = \frac{A_1(x_{31} + x_{24}) + A_2(x_{31} - x_{24})}{12A_0}, \quad y_C - y_0 = \frac{A_1(y_{31} + y_{24}) + A_2(y_{31} - y_{24})}{12A_0}, \\ &x_D - x_0 = -3(x_C - x_0), \quad y_D - y_0 = -3(y_C - y_0), \quad \xi_C = \frac{2A_0A_1}{B_{C1} + \sqrt{12A_0^2A_1^2 + B_{C1}^2}} \approx \frac{A_1}{3A_0}, \\ &\eta_C = \frac{2A_0A_2}{B_{C2} + \sqrt{12A_0^2A_2^2 + B_{C2}^2}} \approx \frac{A_2}{3A_0}, \quad \xi_D = \frac{-2A_0A_1}{A_0^2 + A_1^2 - A_2^2 + \sqrt{B_D}}, \quad \eta_D = \frac{-2A_0A_2}{A_0^2 - A_1^2 + A_2^2 + \sqrt{B_D}}. \end{aligned} \tag{64}$$

in which $B_{C1} = 3A_0^2 - A_1^2 + A_2^2$, $B_{C2} = 3A_0^2 + A_1^2 - A_2^2$ and $B_D = (A_0^2 - A_1^2 - A_2^2)^2 - 4A_1^2A_2^2$. The approximations given for ξ_C and η_C become exact if either $A_1 = 0$ or $A_2 = 0$. For a rectangular or parallellogram geometry $A_1 = A_2 = 0$, and $\xi_C = \eta_C = \xi_D = \eta_D = 0$. This is the origin of the $\{\xi, \eta\}$ system, which lies at the intersection of the two quadrilateral medians. For any other geometry C and D do not lie at the intersection of the medians.

The following ratios appear in the formulation of the higher-order-mode pass filter matrix introduced in §3.8:

$$\begin{aligned} H_1 &= (A_0 + A_1 + A_2)/(2A_0) = A_{234}/A_0, \quad H_2 = (-A_0 + A_1 - A_2)/(2A_0) = -A_{341}/A_0, \\ H_3 &= (A_0 - A_1 - A_2)/(2A_0) = A_{412}/A_0, \quad H_4 = (-A_0 - A_1 + A_2)/(2A_0) = -A_{123}/A_0. \end{aligned} \tag{65}$$

The following metric coefficients are ubiquitous:

$$\begin{aligned} J_1^2 &= (\partial x/\partial\xi)^2 + (\partial y/\partial\xi)^2 = J_{11}^2 + J_{12}^2 = \tfrac{1}{4}L_{68}^2 + \tfrac{1}{8}(L_{43}^2 - L_{21}^2)\eta + \tfrac{1}{8}(L_{21}^2 + L_{43}^2 - 2L_{68}^2)\eta^2, \\ J_2^2 &= (\partial x/\partial\eta)^2 + (\partial y/\partial\eta)^2 = J_{21}^2 + J_{22}^2 = \tfrac{1}{4}L_{75}^2 + \tfrac{1}{8}(L_{32}^2 - L_{14}^2)\xi + \tfrac{1}{8}(L_{14}^2 + L_{32}^2 - 2L_{75}^2)\xi^2. \end{aligned} \tag{66}$$

Here L_{75} and L_{68} denote the median lengths; see number labels in Figure 16(b). By convention we take $J_1 = +\sqrt{J_1^2}$ and $J_2 = +\sqrt{J_2^2}$. The following definitions simplify several subsequent formulas:

$$\begin{aligned} &\cos\phi_1 = \frac{J_{11}}{J_1}, \quad \sin\phi_1 = \frac{J_{12}}{J_1}, \quad \sin\phi_2 = -\frac{J_{21}}{J_2}, \quad \cos\phi_2 = \frac{J_{22}}{J_2}, \\ &J = J_{11}J_{22} - J_{12}J_{21} = J_1\,J_2\,(\cos\phi_1\cos\phi_2 + \sin\phi_1\sin\phi_2) = J_1\,J_2\,\cos(\phi_1{-}\phi_2). \\ &\mathbf{D}_J = \begin{bmatrix} 1/J_1 & 0 \\ 0 & 1/J_2 \end{bmatrix}, \quad \mathbf{D}_{JJ} = \begin{bmatrix} 1/J_1^2 & 0 & 0 \\ 0 & 1/J_2^2 & 0 \\ 0 & 0 & 1/(J_1J_2) \end{bmatrix}, \\ &\breve{\mathbf{J}} = \mathbf{D}_J\mathbf{J} = \begin{bmatrix} J_{11}/J_1 & J_{12}/J_1 \\ J_{21}/J_2 & J_{22}/J_2 \end{bmatrix} = \begin{bmatrix} \cos\phi_1 & \sin\phi_1 \\ -\sin\phi_2 & \cos\phi_2 \end{bmatrix}, \quad \det(\breve{\mathbf{J}}) = \cos(\phi_1{-}\phi_2) = J/(J_1\,J_2). \end{aligned} \tag{67}$$

The physical significance of the angles ϕ_1 and ϕ_2 is illustrated in Figure 5(a).

A.3 Geometric Invariants

Quadratic combinations of A_0, A_1 and A_2 may be express rationally in terms of the squared lengths of sides and diagonals. The following formulas were found by *Mathematica*:

$$\begin{aligned} 4A_0^2 &= L_{31}^2L_{42}^2 - \tfrac{1}{4}P^2, \quad 16A_1^2 = 4L_{21}^2L_{43}^2 - (L_{14}^2 + L_{32}^2 - L_{31}^2 - L_{42}^2)^2, \\ 16A_2^2 &= 4L_{14}^2L_{32}^2 - (L_{21}^2 + L_{43}^2 - L_{31}^2 - L_{42}^2)^2, \quad 16A_0A_1 = (L_{32}^2 - L_{14}^2)P + L_{31}^2Q + L_{42}^2R, \\ 16A_0A_2 &= (L_{21}^2 - L_{43}^2)P - L_{31}^2Q + L_{42}^2R, \\ 16A_1A_2 &= -((2L_{31}^2Q - 2L_{42}^2R + P(-Q+R))(2L_{31}^2Q + 2L_{42}^2R + P(Q+R)))/(16A_0^2), \end{aligned} \tag{68}$$

in which

$$\begin{aligned} P &= L_{21}^2 - L_{32}^2 + L_{43}^2 - L_{14}^2, \qquad Q = L_{21}^2 + L_{32}^2 - L_{43}^2 - L_{14}^2, \\ R &= -L_{21}^2 + L_{32}^2 + L_{43}^2 - L_{14}^2, \quad S = L_{21}^2 + L_{32}^2 + L_{43}^2 + L_{14}^2, \\ L_{21}^2 &= \tfrac{1}{4}(P + Q - R + S), \qquad L_{32}^2 = \tfrac{1}{4}(-P + Q + R + S), \\ L_{43}^2 &= \tfrac{1}{4}(P - Q + R + S), \qquad L_{14}^2 = \tfrac{1}{4}(-P - Q - R + S). \end{aligned} \tag{69}$$

The first of (68) is Bratschneider's 1842 formula, see http://mathworld.wolfram.com/Quadrilateral.com. It is not known if the others are new. The geometry of an arbitrary quadrilateral is defined by five independent quantities. It is convenient to pick invariants. For example, the four side lengths and one diagonal length could be selected, but this is not symmetric as regards choice of diagonal. A more balanced choice consists of taking the three invariants A_0, A_1, A_2 plus the semisum and semidifference of the squared diagonal lengths: $K_1 = \frac{1}{2}(L_{31}^2 + L_{42}^2)$

and $K_2 = \frac{1}{2}(L_{31}^2 - L_{42}^2)$. We get

$$
\begin{aligned}
P &= -\sqrt{L_{31}L_{42} - 4A_0^2} = -\sqrt{K_1^2 - K_2^2 - 4A_0^2}, \\
Q &= \frac{(2A_1(K_1 - K_2 - P) - 2A_2(K_1 - K_2 + P)}{A_0}, \quad R = \frac{(2A_1(K_1 + K_2 - P) - 2A_2(K_1 + K_2 + P)}{A_0}, \\
S &= 2\frac{4A_0^2(K_1K_2 - 4A_1A_2) + (2A_2K_2 + 2A_1K_1 - 2A_1P)(2A_1K_2 + 2A_2K_1 + 2A_2P)}{4A_0^2K_2},
\end{aligned}
\tag{70}
$$

The squared median lengths can also be expressed in terms of invariants. The following relations were discovered by *Mathematica*:

$$
\begin{aligned}
L_{57}^2 &= \tfrac{1}{4}(L_{42}^2 + L_{31}^2 - L_{21}^2 + L_{32}^2 - L_{43}^2 + L_{14}^2) = \tfrac{1}{2}(K_1 - P) \\
L_{68}^2 &= \tfrac{1}{4}(L_{42}^2 + L_{31}^2 + L_{21}^2 - L_{32}^2 + L_{43}^2 - L_{14}^2) = \tfrac{1}{2}(K_1 + P)
\end{aligned}
\tag{71}
$$

It follows that $L_{68}^2 + L_{75}^2 = \frac{1}{2}(L_{31}^2 + L_{42}^2)$, which is a well known property.

Acknowledgements

Preparation of this paper has been partly supported by the National Science Foundation under Grant CMS–0219422, and partly by the Finite Elements for Salinas contract with Sandia National Laboratories.

References

[1] D. J. Allman, Evaluation of the constant strain triangle with drilling rotations, *Int. J. Numer. Meth. Engrg.*, **26**, 2645–2655, 1988.

[2] K. Alvin, H. M. de la Fuente, B. Haugen and C. A. Felippa, Membrane triangles with corner drilling freedoms: I. The EFF element, *Finite Elem. Anal. Des.*, **12**, 163–187, 1992.

[3] J. H. Argyris and S. Kelsey, *Energy Theorems and Structural Analysis*, London, Butterworths, 1960. Part I reprinted from *Aircr. Engrg.*, **26**, Oct-Nov 1954 and **27**, April-May 1955.

[4] J. H. Argyris, S. Kelsey, and H. Kamel, H., Matrix methods of structural analysis — a precis of recent developments, in *AGARDograph 72: Matrix Methods of Structural Analysis*, ed. by B. M. Fraeijs de Veubeke, Pergamon Press, Oxford, 1–164, 1964.

[5] J. H. Argyris, Continua and discontinua, in *Proc. 1st Conf. Matrix Meth. Struc. Mech.*, ed. by J. Przemieniecki et. al., AFFDL-TR-66-80, Air Force Institute of Technology, Dayton, Ohio, 10–170, 1965.

[6] T. Belytschko, W. K. Liu and B. E. Engelmann, The gamma elements and related developments, in T. J. R. Hughes and E. Hinton (eds.), *Finite Element Methods for Plate and Shell Structures, Vol. I: Element Technology*, Pineridge Press, Swansea, U.K., 316–347, 1986.

[7] P. G. Bergan and L. Hanssen, A New Approach for Deriving 'Good' Finite Elements, in *The Mathematics of Finite Elements and Applications – Volume II*, ed. by J. R. Whiteman, Academic Press, London, 483–497, 1976.

[8] P. G. Bergan, Finite elements based on energy orthogonal functions, *Int. J. Numer. Meth. Engrg.*, **15**, 1141–1555, 1980.

[9] P. G. Bergan and M. K. Nygård, Finite elements with increased freedom in choosing shape functions, *Int. J. Numer. Meth. Engrg.*, **20**, 643–664, 1984.

[10] P. G. Bergan and C. A. Felippa, A triangular membrane element with rotational degrees of freedom, *Comp. Meths. Appl. Mech. Engrg.*, **50**, 25–69, 1985.

[11] P. G. Bergan and C. A. Felippa, Efficient implementation of a triangular membrane element with drilling freedoms, in T. J. R. Hughes and E. Hinton (eds.), *Finite Element Methods for Plate and Shell Structures, Vol. I: Element Technology*, Pineridge Press, Swansea, U.K., 128–152, 1986.

[12] R. W. Clough, The finite element method – a personal view of its original formulation, in *From Finite Elements to the Troll Platform – the Ivar Holand 70th Anniversary Volume*, ed. by K. Bell, Tapir, Norway, 89–100, 1994.

[13] W. P. Doherty, E. L. Wilson and R. L. Taylor, Stress analysis of axisymmetric solids utilizing higher order quadrilateral finite elements, SESM Report 69-3, Department of Civil Engineering, University of California, Berkeley, 1969.

[14] C. A. Felippa and P. G. Bergan, A triangular plate bending element based on an energy-orthogonal free formulation, *Comp. Meths. Appl. Mech. Engrg.*, **61**, 129–160, 1987.

[15] C. A. Felippa, The extended free formulation of finite elements in linear elasticity, *J. Appl. Mech.*, **56**, 609–616, 1989.

[16] C. A. Felippa and C. Militello, Membrane triangles with corner drilling freedoms: II. The ANDES element, *Finite Elem. Anal. Des.*, **12**, 189–201, 1992.

[17] C. A. Felippa and S. Alexander, Membrane triangles with corner drilling freedoms: III. Implementation and performance evaluation, *Finite Elem. Anal. Des.*, **12**, 203–239, 1992.

[18] C. A. Felippa, A survey of parametrized variational principles and applications to computational mechanics, *Comp. Meths. Appl. Mech. Engrg.*, **113**, 109–139, 1994.

[19] C. A. Felippa, B. Haugen and C. Militello, From the individual element test to finite element templates: evolution of the patch test, *Int. J. Numer. Meth. Engrg.*, **38**, 199–222, 1995.

[20] C. A. Felippa, Parametrized unification of matrix structural analysis: classical formulation and d-connected mixed elements, *Finite Elem. Anal. Des.*, **21**, 45–74, 1995.

[21] C. A. Felippa, Recent developments in parametrized variational principles for mechanics, *Comput. Mech.*, **18**, 159–174, 1996.

[22] C. A. Felippa and C. Militello, Construction of optimal 3-node plate bending elements by templates, *Comput. Mech.*, **24**, 1–13, 1999.

[23] C. A. Felippa, Recent developments in basic finite element technologies, in *Computational Mechanics in Structural Engineering-Recent Developments*, ed. by F.Y. Cheng and Y. Gu, Elsevier, Amsterdam, 141–156, 1999.

[24] C. A. Felippa, Recent advances in finite element templates, in *Computational Mechanics for the Twenty-First Century*, ed. by B.J.V. Topping, Saxe-Coburn Pub., Edinburgh, 71–98, 2000.

[25] C. A. Felippa and K. C. Park, Fitting strains and displacements by minimizing dislocation energy, Proceedings of the Sixth International Conference on Computational Structures Technology, Prague, Czech Republic, 49–51, 2002. Complete text in CDROM. Available from: http://caswww.colorado.edu/Felippa.d/FelippaHome.d/Publications.d/Report.CU-CAS-02-25.pdf

[26] C. A. Felippa, A study of optimal membrane triangles with drilling freedoms, *Comp. Meths. Appl. Mech. Engrg.*, **192**, 2125–2168, 2003.

[27] C. A. Felippa, A template tutorial, Chapter 3 in *Computational Mechanics: Theory and Practice*, ed. by K. M. Mathisen, T. Kvamsdal and K. M. Okstad, CIMNE, Barcelona, 29–68, 2004. Available from: http://caswww.colorado.edu/Felippa.d/FelippaHome.d/Publications.d/Report.CU.CAS-05-04.pdf

[28] R. H. Gallaguer, *A Correlation Study of Methods of Matrix Structural Analysis*, Pergamon Press, Oxford, 1964.

[29] L. Hanssen, P. G. Bergan and T. J. Syversten, Stiffness derivation based on element convergence requirements, in *The Mathematics of Finite Elements and Applications – Volume III*, ed. by J. R. Whiteman, Academic Press, London, 83–96, 1979.

[30] T. J. R. Hughes and D. S. Malkus, Mixed finite element methods – reduced and selective integration techniques: a unification of concepts, *Comp. Meths. Appl. Mech. Engrg.*, bf 15, 63–81, 1978.

[31] T. J. R. Hughes, Generalization of selective integration procedures to anisotropic and nonlinear media, *Int. J. Numer. Meth. Engrg.*, **15**, 1413–148, 1980.

[32] T. J. R. Hughes and D. S. Malkus, A general penalty mixed equivalence theorem for anisotropic, incompressible finite elements, in *Hybrids and Mixed Finite Element Methods*, ed. by S. N. Atluri, R. H. Gallagher and O. C. Zienkiewicz, Wiley, London, 1983.

[33] T. J. R. Hughes, *The Finite Element Method: Linear Static and Dynamic Finite Element Analysis*, Prentice Hall, Englewood Cliffs, N. J., 1987. Reprinted by Dover, NY, 2000.

[34] B. M. Irons, Engineering application of numerical integration in stiffness methods, *AIAA J.*, **4**, pp. 2035–2037, 1966.

[35] B. M. Irons and S. Ahmad, *Techniques of Finite Elements*, Ellis Horwood Ltd, Chichester, UK, 1980.

[36] K. Kavanagh and S. W. Key, A note on selective and reduced integration techniques in the finite element method, *Int. J. Numer. Meth. Engrg.*, **4**, 148–150, 1972.

[37] N. Lautersztajn-S and A. Samuelsson, Further discussion on four-node isoparametric elements in plane bending, *Int. J. Numer. Meth. Engrg.*, **47**, 129–140, 2000.

[38] R. H. MacNeal, A simple quadrilateral shell element, *Computers & Structures*, **8**, 175–183, 1978.

[39] R. H. MacNeal and R. L. Harder, A proposed standard set of problems to test finite element accuracy, *Finite Elem. Anal. Des.*, **1**, 3–20, 1985.

[40] R. H. MacNeal, The evolution of lower order plate and shell elements in MSC/NASTRAN, in T. J. R. Hughes and E. Hinton (eds.), *Finite Element Methods for Plate and Shell Structures, Vol. I: Element Technology*, Pineridge Press, Swansea, U.K., 85–127, 1986.

[41] R. H. MacNeal, A theorem regarding the locking of tapered four noded membrane elements, *Int. J. Numer. Meth. Engrg.*, **24**, 1793–1799, 1987.

[42] R. F. Melosh, Development of the stiffness method to define bounds on the elastic behavior of structures, *Ph.D. Dissertation*, University of Washington, Seattle, 1962.

[43] R. F. Melosh, Bases for the derivation of matrices for the direct stiffness method, *AIAA J.*, **1**, 1631–1637, 1963.

[44] C. Militello and C. A. Felippa, The First ANDES Elements: 9-DOF Plate Bending Triangles, *Comp. Meths. Appl. Mech. Engrg.*, **93**, 217–246, 1991.

[45] C. Militello and C. A. Felippa, The individual element patch revisited, in *The Finite Element Method in the 1990's — a book dedicated to O. C. Zienkiewicz*, ed. by E. Oñate, J. Periaux and A. Samuelsson, CIMNE, Barcelona and Springer-Verlag, Berlin, 554–564, 1991.

[46] M. K. Nygård, The Free Formulation for nonlinear finite elements with applications to shells, *Ph. D. Dissertation*, Division of Structural Mechanics, NTH, Trondheim, Norway, 1986.

[47] K. C. Park and G. M. Stanley, A curved C^0 shell element based on assumed natural-coordinate strains, *J. Appl. Mech.*, **53**, 278–290, 1986.

[48] S. F. Pawsey and R. W. Clough, Improved numerical integration of thick shell finite elements, *Int. J. Numer. Meth. Engrg.*, **3**, 545–586, 1971.

[49] T. H. H. Pian, Derivation of element stiffness matrices by assumed stress distributions, *AIAA J.*, **2**, 1333–1336, 1964.

[50] T. H. H. Pian, Element stiffness matrices for boundary compatibility and for prescribed boundary stresses, in *Proc. 1st Conf. on Matrix Methods in Structural Mechanics*, AFFDL-TR-66-80, Air Force Institute of Technology, Dayton, Ohio, 457–478, 1966.

[51] T. H. H. Pian and P. Tong, Basis of finite element methods for solid continua, *Int. J. Numer. Meth. Engrg.*, **1**, 3–29, 1969.

[52] T. H. H. Pian and K. Sumihara, Rational approach for assumed stress finite elements, *Int. J. Numer. Meth. Engrg.*, **20**, 1685–1695, 1984.

[53] T. H. H. Pian, Some notes on the early history of hybrid stress finite element method, *Int. J. Numer. Meth. Engrg.*, **47**, 419–425, 2000.

[54] J. C. Simo and M. S. Rifai, A class of mixed assumed strain methods and the method of incompatible modes, *Int. J. Numer. Meth. Engrg.*, **29**, 1595–1638, 1990.

[55] G. Skeie, The Free Formulation: linear theory and extensions with applications to tetrahedral elements with rotational freedoms, *Ph. D. Dissertation*, Division of Structural Mechanics, NTH, Trondheim, Norway, 1991.

[56] G. Strang, Variational crimes in the finite element method, in *The Mathematical Foundations of the Finite Element Method with Applications to Partial Differential Equations*, ed. by A. K. Aziz, Academic Press, New York, 689–710, 1972.

[57] G. Strang and G. Fix, *An Analysis of the Finite Element Method*. Prentice-Hall, 1973.

[58] G. M. Stanley, K. C. Park and T. J. R. Hughes, Continuum based resultant shell elements, in T. J. R. Hughes and E. Hinton (eds.), *Finite Element Methods for Plate and Shell Structures, Vol. I: Element Technology*, Pineridge Press, Swansea, U.K., 1–45, 1986.

[59] I. C. Taig and R. I. Kerr, Some problems in the discrete element representation of aircraft structures, in *Matrix Methods of Structural Analysis*, ed. by B. M. Fraeijs de Veubeke, Pergamon Press, London, 1964.

[60] R. L. Taylor, E. L. Wilson and P. J. Beresford, A nonconforming element for stress analysis, *Int. J. Numer. Meth. Engrg.*, **10**, 1211–1219, 1976.

[61] M. J. Turner, R. W. Clough, H. C. Martin and L. J. Topp, Stiffness and deflection analysis of complex structures, *J. Aero. Sci.*, **23**, 805–824, 1956.

[62] E. L. Wilson, R. L. Taylor, W. P. Doherty and J. Ghaboussi, Incompatible displacement models, in *Numerical and Computer Models in Structural Mechanics*, ed. by S. J. Fenves, N. Perrone, A. R. Robinson and W. C. Schnobrich, Academic Press, New York, 43–57, 1973.

[63] C. C. Wu and Y. K. Cheung, On optimization approaches of hybrid stress elements, *Finite Elem. Anal. Des.*, **21**, 111–128, 1995.

[64] O. C. Zienkiewicz, R. L. Taylor and J. M. Too, Reduced integration technique in general analysis of plates and shells, *Int. J. Numer. Meth. Engrg.*, **3**, 275–290, 1971.